Journal of Volcanology and Geothermal Research 376 (2019) 27–43

Contents lists available at ScienceDirect

Journal of Volcanology and Geothermal Research

journal homepage: www.elsevier.com/locate/jvolgeores

Age of the dacite of Sunset Amphitheater, a voluminous Pleistocene tephra from Mount Rainier (USA), and implications for Cascade glacial stratigraphy

Thomas W. Sisson [a,*], Axel K. Schmitt [b], Martin Danišík [c], Andrew T. Calvert [a], Napoleon Pempena [d], Chun-Yuan Huang [e,f], Chuan-Chou Shen [e,f]

[a] United States Geological Survey, Volcano Science Center, Menlo Park, USA
[b] Institut für Geowissenschaften, Universität Heidelberg, Im Neuenheimer Feld 234-236, D-61920 Heidelberg, Germany
[c] John de Laeter Centre, TIGeR, School of Earth and Planetary Sciences, Curtin University, Perth, Australia
[d] Department of Earth, Planetary & Space Sciences, University of California, Los Angeles, USA
[e] High-Precision Mass Spectrometry and Environment Change Laboratory (HISPEC), Department of Geosciences, National Taiwan University, Taipei 10617, Taiwan, ROC
[f] Research Center for Future Earth, National Taiwan University, Taipei 10617, Taiwan, ROC

ARTICLE INFO

Article history:
Received 5 September 2018
Received in revised form 28 February 2019
Accepted 5 March 2019
Available online 7 March 2019

Keywords:
Pleistocene
$^{40}Ar/^{39}Ar$
Plagioclase
(U-Th)/He
Zircon
Tephra
Till
Marine isotope stage
Puget Sound

ABSTRACT

The dacite of Sunset Amphitheater, Mount Rainier (USA), illustrates the difficulties in establishing accurate ages of Pleistocene tephra eruptions. Nearly uniform whole-rock, glass, and mineral compositions, texture, and phenocryst assemblage establish that certain conspicuous dissected pumice exposures scattered from Mount Rainier to southern Puget Sound are products of the same Pleistocene Plinian eruption. Deposit thicknesses and pumice sizes support an eruption on the order of low Volcanic Explosivity Index (VEI) 5, atypically explosive for dominantly lava-producing Mount Rainier. Statistically permissible $^{40}Ar/^{39}Ar$ plateau ages of plagioclase phenocryst separates are 138 ± 20 ka and 101 ± 11 ka (2σ). A previously published result of 206 ± 11 ka is herein shown to result from a sample selection error. Zircon from the pumice yields a U-Th crystallization age of 147 ± 8 ka if the isochron is required to pass through the tephra U-Th isotopic composition. In contrast, pooled (U-Th)/He measurements on the zircon yield an age of 85 ± 6 ka (2σ), which accords with well-behaved $^{40}Ar/^{39}Ar$ ages of stratigraphically associated lavas high on Mount Rainier, and is the best estimate of the pumice's true eruption age. Inclusions of undegassed melt (glass) in the plagioclase separates are proposed as biasing apparent $^{40}Ar/^{39}Ar$ plateau ages to old values through coupling of undegassed magmatic excess Ar with radiogenic Ar that accumulated post-eruptively from relatively K-rich glass. U-Th ages record zircon growth prior to eruption, consistent with a possible complex history of advanced solidification followed by remobilization. The ca. 85 ka eruption age confirms that bracketing glacial tills on the flanks of Mount Rainier were products of the Penultimate Glaciation (MIS 6) and Last Glacial Maximum (MIS 2). This eruption age also provides an important time marker for glacial and other sedimentary deposits in southern Puget Sound lowland that, excepting the Vashon Drift (MIS 2), generally lack reliable age determinations.

Published by Elsevier B.V.

1. Introduction

It is useful to know the ages of explosive eruptions for many reasons, including anticipating and quantifying hazards, understanding magmatic and volcanic processes, assessing the eruptions' influences on the environment, and as time markers for other geologic events. Holocene explosive eruptions can be straightforward to date, whereas those from the Pleistocene can be distinctly challenging. In both cases, the eruption deposits can be distributed widely, and for the Holocene one place or another can usually be found where twigs, wood, or peat overlie, underlie, or are contained within a particular tephra fall that can provide reliable ^{14}C ages. Conversely for the Pleistocene, erosion has dissected much of the deposits, organic decay has destroyed materials suitable for ^{14}C dating, and many such deposits are too old for the ^{14}C method to yield usefully precise ages. The K-Ar and $^{40}Ar/^{39}Ar$ dating methods can be of restricted utility due to a common absence of alkali feldspar phenocrysts, and due to quenching of the melt to vesicular glass that remains open to hydration and other chemical exchange. Plagioclase phenocrysts are common in tephras from magmatic arcs and continental interiors, and these can yield accurate and usefully precise $^{40}Ar/^{39}Ar$ ages, but their low K concentrations make such age measurements susceptible to the presence of glass and vapor inclusions. Such inclusions can be quite small and impractical-to-impossible to remove

* Corresponding author.
E-mail address: tsisson@usgs.gov (T.W. Sisson).

https://doi.org/10.1016/j.jvolgeores.2019.03.003
0377-0273/Published by Elsevier B.V.

entirely from plagioclase separates, some glass inclusions may not be sealed and so are open to chemical exchange with the environment, and glass and vapor inclusions that are sealed can contain excess ^{40}Ar, collectively leading to complex $^{40}Ar/^{39}Ar$ age spectra.

Zircon is a complementary or alternative target for determining the ages of explosively produced tephras and of other geologic materials. In-situ dating of zircon by secondary ion mass spectroscopy (SIMS) and by laser-ablation inductively coupled plasma mass spectrometry (LA-ICP-MS) allow targeting of late-grown zones (e.g. grain surfaces and rims) and are yielding useful ages into the Pleistocene via the U-Pb and U-Th decay systems (e.g., Reid et al., 1997; Danišík et al., 2012; Matthews et al., 2015; Coble et al., 2017; Avellán et al., 2018). Due to slow diffusion within zircon and of zircon components through melt, U-Pb and U-Th ages of zircon can nevertheless date events older to much older than those that immediately preceded a particular explosive eruption. While such ages have their uses, they can be misleading as to the actual eruption age. In contrast, ^{4}He is a decay product of U, Th, and to lesser extent Sm that diffuses quickly through zircon and other minerals until they cool to substantially sub-magmatic temperatures (Reiners et al., 2004). As such, the (U-Th)/He method can provide reliable eruption ages for tephras under the conditions that zircon grains are present, are sufficiently coarse and reasonably homogeneous in their distribution of Th and U such that ejection of radiogenic ^{4}He from the grain surface can be accounted for, and that corrections for initial U-Th disequilibrium can be performed reliably (Farley et al., 2002; Schmitt et al., 2012; Danišík et al., 2017).

Herein, we report a case study dating a sizeable Pleistocene dacite pumice deposit that erupted explosively from Mount Rainier in the Cascade Range of Washington State, USA (Fig. 1). This tephra, the dacite of Sunset Amphitheater, is one of two atypically voluminous pumiceous fall deposits known to have erupted from Mount Rainier in the Pleistocene. As such, it is a potential time-stratigraphic marker in the Pacific Northwest, and it is of interest for understanding abnormally explosive behavior at Mount Rainier and at similar lava-dominated andesitic volcanoes. Mount Rainier grew to be the tallest volcano of the Cascades (4392 m) mainly by effusive eruptions of andesite through low-SiO_2 dacite lavas (Fiske et al., 1963; Sisson et al., 2014) accompanied by small-volume, sparsely vesicular, but glassy tephra that form thin (cm-sized in thickness) fall deposits near the volcano (Sisson and Vallance, 2009). Rarely, Mount Rainier erupted pumiceous tephra, the largest in the Holocene being the sub-Plinian C deposit of 2200 yr BP (Mullineaux, 1974) with a volume of only about 0.11 km^3 (0.03 km^3 DRE) (Nathenson, 2017) and a Volcanic Explosivity Index (VEI) just above the boundary from 3 to 4. Two much thicker and coarser pumiceous fall deposits are known from Pleistocene Mount Rainier, one being a biotite-bearing rhyodacite preserved as a narrow strip of exposures about 12 km east-northeast of the volcano's summit (Sisson et al., 2014), and the other, which is the subject of this report, consisting of dacite pumice exposed prominently in the headwall of Sunset Amphitheater on the volcano's upper west flank (Figs. 2, 3) as well as at least four other localities (described in the following) as distant from the volcano as southern Puget Sound (Figs. 1, 2).

Large glaciers presently descend Mount Rainier to as low as 1150 m elevation, and larger glaciers deeply filled the surrounding valleys over much of the Pleistocene, as shown by ice-contact features on the sides of ridge-capping Mount Rainier lava flows situated high above valley floors (Lescinsky and Sisson, 1998) and by widespread slope-mantling tills (Crandell and Miller, 1974). As a result, the dacite of Sunset Amphitheater's deposit is highly dissected, precluding construction of isopach maps. Nevertheless, deposit thicknesses on the order of 2 m at exposures 8–15 km east-northeast from the volcano's summit vent, with maximum pumice sizes of about 6–8 cm at that distance, are between those of Mount St. Helens' Holocene Wn and Yn tephras along their deposit axes (Carey et al., 1995). Nathenson (2017) reassessed volumes of Holocene and latest Pleistocene pumiceous Cascades tephras and derived 0.7–1.4 km^3 (0.2–0.4 km^3 DRE) for the Wn and 3–8.8 km^3 (0.8–2.3 km^3 DRE) for the Yn. The volume of the dacite of Sunset Amphitheater therefore may have been on the order of one to several km^3 (0.3–0.8 km^3 DRE), but with considerable uncertainty. At that volume range, its causative eruption would classify as low VEI 5.

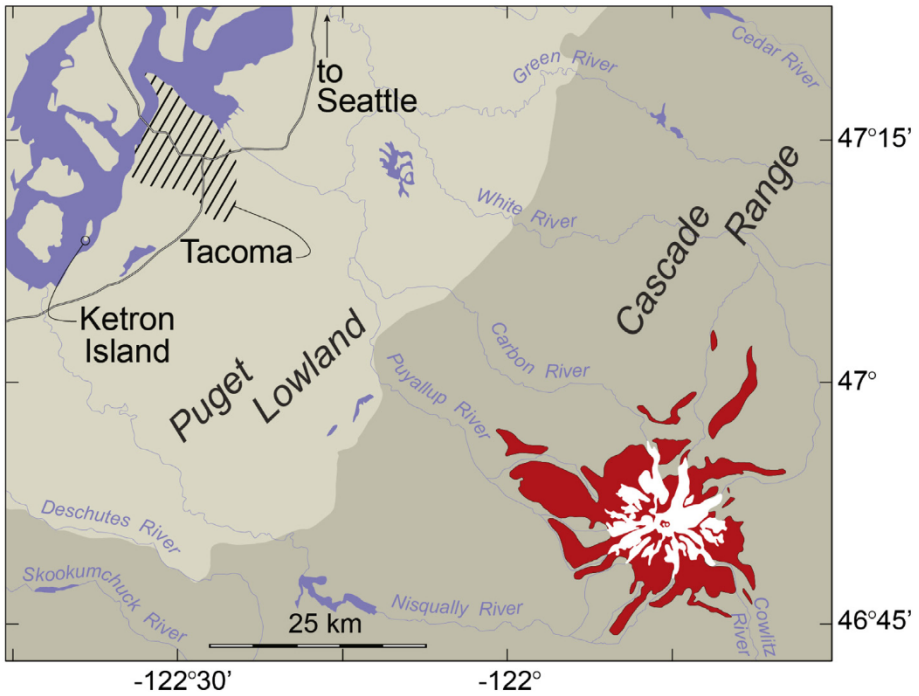

Fig. 1. Map showing the location of Mount Rainier volcanic rocks (red); glaciers (white); rivers, lakes, and southern Puget Sound (blue); Cascade Range (dark tan); Puget Lowland (light tan); major highways (black and white lines); and the Tacoma metropolitan area (diagonal lines). The south end of Ketron Island exposes cross-bedded sands rich in pumice of the dacite of Sunset Amphitheater. Inset shows map location in the North American Pacific Northwest with summits of major volcanoes marked as diamonds.

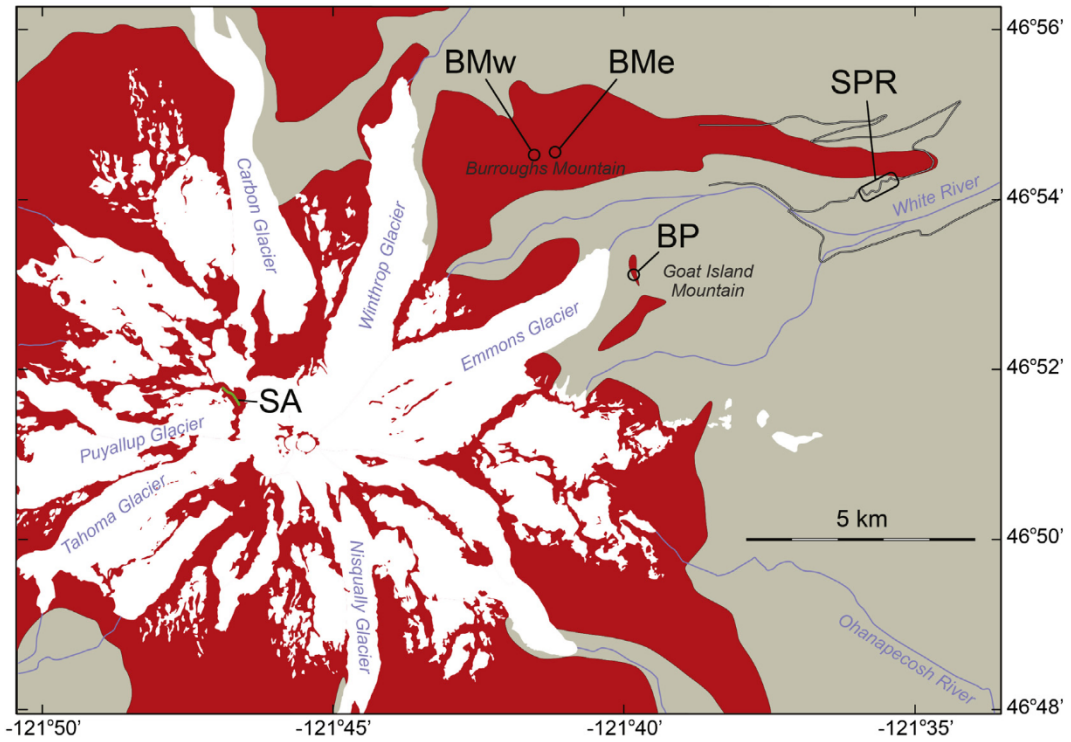

Fig. 2. Map showing known exposures of the dacite of Sunset Amphitheater close to Mount Rainier. Green line (SA) is the pumice band in Sunset Amphitheater Headwall. Other locations are Baker Point (BP), Sunrise Park Road (SPR), and the east and west sides of Burroughs Mountain (BMe, BMw). Pleistocene volcanic rocks and glaciers of Mount Rainier are shown as red and white, respectively. Tertiary volcanic rocks are shown as tan, and rivers as blue. Paved roads in the White River valley and to Sunrise Park are shown as black and white lines.

This report describes the dacite of Sunset Amphitheater and its known exposures, along with a compilation of whole-rock, mineral and glass compositional data. It also recounts a succession of attempts to date the pumice beginning with $^{40}Ar/^{39}Ar$ on plagioclase phenocrysts, then U-Th on zircon, and ending with (U-Th)/He on zircon. Apparent ages are progressively younger with these methods, but the (U-Th)/He age is consistent with $^{40}Ar/^{39}Ar$ ages of stratigraphically associated nearby lava flows high on the volcano. A preliminary but erroneously old $^{40}Ar/^{39}Ar$ age interpretation for the tephra was used in three publications (Walsh et al., 2003a, 2003b; John et al., 2008); this report corrects that error and outlines the value of the revised eruption age for understanding volcanic and glacial histories of the Cascade Range and Puget Lowland.

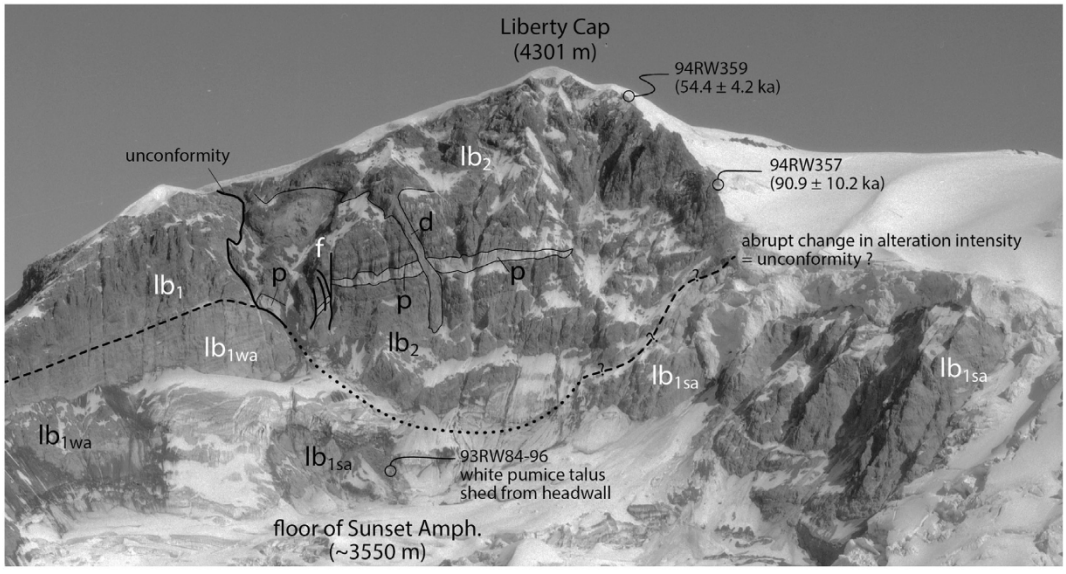

Fig. 3. Photo looking north-northeast toward Sunset Amphitheater annotated with geologic details. Lavas and breccias below an unconformity are labeled: lb_1 and are further subdivided into non-altered (no additional subscript), weakly altered: lb_{1wa}, and strongly altered: lb_{1sa}. Lavas and breccias above the unconformity are labeled: lb_2, the Sunset Amphitheater pumice band: p, and a dike (d) that fed a ridge-crest lava flow. Faults (heavy black lines, f) offset the pumice band down to the northwest. The unconformity in the lower southeast part of the headwall (lower right) is located based on an abrupt change in degree of alteration, but was not visited, and so is shown as queried. A disconformity appears to separate altered and non-altered rocks below the unconformity and is shown by a dashed line (left). Locations, sample numbers, and plateau $^{40}Ar/^{39}Ar$ ages with 95% confidence windows are shown for lavas along Liberty Cap's south-southeast ridge. Base photo is image 92R1–162 taken by R. Krimmel, USGS, on 6 October 1992.

Table 1
Chemical compositions of single pumices and separated glasses (G), dacite of Sunset Amphitheater, normalized anhydrous.

Sample	93RW84	93RW85	93RW86	93RW87	93RW88	93RW89	93RW90	93RW91	93RW92	93RW93	93RW94
Lat	46.860	46.860	46.860	46.860	46.860	46.860	46.860	46.860	46.860	46.860	46.860
Long	−121.781	−121.781	−121.781	−121.781	−121.781	−121.781	−121.781	−121.781	−121.781	−121.781	−121.781
Locality	SA	SA	SA	SA	SA	SA	SA	SA	SA	SA	SA
SiO_2	66.8	66.4	66.0	66.7	67.3	65.9	66.5	66.5	66.6	66.3	67.1
TiO_2	0.61	0.62	0.64	0.60	0.59	0.64	0.63	0.63	0.61	0.62	0.61
Al_2O_3	16.1	16.1	16.3	16.1	16.0	16.3	16.2	16.1	16.2	16.1	16.1
FeO*	3.57	3.75	3.78	3.58	3.46	3.86	3.63	3.68	3.66	3.70	3.51
MnO	0.07	0.07	0.07	0.07	0.06	0.07	0.07	0.07	0.07	0.07	0.07
MgO	1.94	1.99	1.98	1.91	1.76	2.18	1.86	1.97	2.01	2.05	1.86
CaO	4.22	4.20	4.45	4.30	4.06	4.40	4.24	4.31	4.24	4.42	4.04
Na_2O	3.78	3.83	3.90	3.82	3.84	3.83	3.95	3.83	3.77	3.82	3.81
K_2O	2.73	2.83	2.70	2.76	2.79	2.60	2.72	2.70	2.68	2.70	2.76
P_2O_5	0.17	0.18	0.19	0.18	0.17	0.17	0.18	0.17	0.17	0.18	0.17
Total	94.4	97.0	97.2	96.5	96.4	97.0	96.7	97.0	96.9	96.5	96.7
XRF (ppm)											
Rb	80	86	80	80	82	78	82	82	78	80	85
Sr	365	375	400	370	365	390	380	380	370	385	375
Y	16	19	17	16	18	17	18	18	15	18	20
Zr	180	182	180	178	180	176	184	182	174	172	194
Nb	10	10	12	<10	10	10	10	12	<10	10	14
Ba	570	560	560	570	580	530	550	560	550	550	570
Ni	10	<10	<10	10	<10	12	<10	<10	10	<10	<10
Cu	<10	<10	<10	<10	<10	<10	<10	<10	<10	<10	10
Zn	51	44	50	50	48	53	46	50	50	48	52
Cr	25	22	20	21	<20	26	27	24	32	25	33
V											
Pb											
INAA (ppm)											
Rb	77.4	80.0	76.0	81.0							
Sr	390	400	420	400							
Cs	4.51	4.42	4.31	4.57							
Ba	515	513	500	520							
Th	11.4	11.1	10.9	11.3	12.4	12.0	10.8	11.1	11.2	11.3	11.4
U	3.78	3.61	3.46	3.86	4.47	4.02	4.33	4.23	4.07	4.27	4.32
La	24.1	24.0	23.3	24.3							
Ce	44.7	45.1	45.0	44.9							
Pr											
Nd	17.0	19.0	19.0	19.0							
Sm	3.66	3.77	3.79	3.72							
Eu	0.89	0.93	0.93	0.913							
Gd											
Tb	0.45	0.45	0.48	0.43							
Dy											
Ho											
Er											
Tm											
Yb	1.5	1.4	1.3	1.0							
Lu	0.2	0.21	0.21	0.21							
Zr	180	170	190	150							
Hf	4.3	4.4	4.3	4.46							
Nb											
Ta	1.00	0.98	0.99	1.01							
Sc	8.1	8.42	8.49	7.87							
Cr	27.3	32.4	28	29.6							
Co	9.33	9.59	9.96	9.56							
Ni	26	<17.0	26	17							
Zn	46	46	46	48							
As	2.1	2	2.3	2.2							
Sb	0.32	0.33	0.53	0.94							
Y											
Pb											

Notes: Major oxides are normalized to 100% with all Fe as FeO (FeO*); Total gives original analytical sum; locations are NAD27 CONUS latitude and longitude; localities are SA - Sunset Amphitheater, BP - Baker Point, BM - Burroughs Mountain, KI - Ketron Island

[a] Pumice sample 01SR892 is weathered and clay-rich; Cu and Zn not reported for glass separates due to use of methylene-iodide stabilized with a Cu-Zn coin.

2. Exposures of the dacite of Sunset Amphitheater

2.1. Sunset Amphitheater Headwall (46.8617° N, 121.7800° W)

Sunset Amphitheater is a southwest-facing cirque-like basin at the head of the Puyallup Glacier on the upper west flank of Mount Rainier about 2 km west-northwest of the volcano's summit (Fig. 2). The glacier-filled floor of the amphitheater, at about 3550 m elevation, is about 1.3 km broad in a NW-SE direction. The amphitheater headwall rises steeply (average ~48°, locally vertical) to the 4300 m summit of a spur peak of Mount Rainier known as Liberty Cap (Fig. 3). The headwall largely exposes thin lava flows and concordant bands of breccia and scoriae with shallow westward apparent dips (~7°). The dacite of Sunset Amphitheater crops out as a prominent white band of pumice that

93RW94	93RW95	95SR492B	95SR492A	95SR492C	01SR892[a]	05KI921-1	05KI921-1G	05KI921-2	05KI921-2G
46.860	46.860	46.8862	46.8862	46.8862	46.9095	47.1472	47.1472	47.1472	47.1472
−121.781	−121.781	−121.6625	−121.6625	−121.6625	−121.6858	−122.6377	−122.6377	−122.6377	−122.6377
SA	SA	BP	BP	BP	BM	KI	KI	KI	KI
67.1	66.6	65.8	65.4	66.8	63.8	65.9	74.7	66.5	74.6
0.61	0.64	0.62	0.65	0.58	0.71	0.62	0.29	0.61	0.30
16.1	16.1	17.0	17.2	16.6	18.7	16.4	13.7	16.1	13.7
3.51	3.70	3.73	3.82	3.41	4.10	3.39	1.38	3.30	1.39
0.07	0.07	0.07	0.07	0.06	0.07	0.07	0.03	0.07	0.03
1.86	2.00	1.88	1.89	1.68	2.05	2.09	0.28	1.93	0.29
4.04	4.21	4.16	4.31	4.03	4.29	4.47	1.49	4.21	1.52
3.81	3.81	3.94	3.89	3.99	3.80	3.95	3.96	4.00	3.92
2.76	2.65	2.57	2.49	2.70	2.26	2.59	4.03	2.68	4.01
0.17	0.17	0.20	0.20	0.18	0.23	0.15	0.07	0.15	0.07
96.7	96.0	96.6	96.4	96.9	95.0	96.2	96.7	96.6	97.2
85	83	70		79	65	73.1	116.6	76.3	115.5
375	385	365		358	376	399	164	385	166
20	16	14		13	12	14.1	18.5	15.6	17.7
194	186	181		187	191	161	205	165	200
14	12	11		13	11	8.6	11.2	8.8	11.3
570	550	565		586	512	513	696	534	697
<10	<10	11		10	13	11	2	10	<1
10	<10	18		18	17	6.8		10.1	
52	52	54		54	50	55		52	
33	<20				24	35	2	25	3
					59	70	17	69	21
					15	13	18	12	19
						ICPMS (ppm)			
			73.4			71.1	121.1	75.6	120.9
			420			390	170	377	174
			4.44			4.39	7.32	4.63	7.27
			579			521	732	539	725
11.4	10.1		12.1			10.9	18.3	11.6	18.3
4.32	4.38		4.73			3.92	6.46	4.15	6.47
			25.7			23.5	31.0	24.3	31.2
			51.9			45.9	59.6	47.2	59.6
						5.33	6.61	5.45	6.62
			22.9			19.6	23.4	19.9	23.3
			4.81			3.93	4.47	3.91	4.35
			1.04			1.07	0.84	1.07	0.81
			3.94			3.22	3.63	3.30	3.61
			0.50			0.50	0.58	0.51	0.57
						2.87	3.28	2.89	3.284
						0.56	0.67	0.57	0.65
						1.50	1.82	1.52	1.78
			0.25			0.22	0.27	0.22	0.27
			1.61			1.38	1.73	1.40	1.71
			0.24			0.22	0.28	0.22	0.27
			171			156	223	162	219
			4.96			4.51	6.28	4.68	6.13
						9.2	11.3	9.5	11.2
			1.11			0.84	1.15	0.88	1.14
			8.87			8.06	4.17	7.98	4.19
			27.1						
			9.87						
			10.9						
			42.9						
			1.89						
			0.27						
						14.4	17.6	14.7	17.5
						11.7	17.4	12.2	17.5

traverses the face for about 0.5 km at slightly less than half the height of the headwall (base of pumice deposit at about 3900 m in the west rising to about 3960 m in the east). The white pumice band reaches a maximum thickness of about 20 m in the steepest part of the headwall, thinning gradually to the west and east. The pumice band pinches out in the eastern third of the headwall and fails to reach the headwall's southeast edge. The pumice band and the volcanic rocks immediately beneath and above it overlie a steep unconformity exposed in the western third of the headwall, near which the pumice is also cut and offset by a series of near-vertical faults with down-to-the-west displacements. A prominent vertical dike also cuts the pumice band; at its top this dike merges with and fed one of the lava flows that crops out on the amphitheater's upper southwest margin. Volcanic rocks exposed shortly below the unconformity vary in their degree of alteration from fresh in the west to strongly altered in the east, as well as being strongly altered in isolated exposures through the glacier below the headwall, to the extent that

flow bases, tops, and igneous mineralogy are difficult to recognize, whereas rocks above the unconformity, including the pumice band, are oxidized where scoriaceous, but are otherwise generally fresh. The pumice was sampled as individual pyroclasts up to about 10 cm across from debris shed onto the glacier from the headwall; larger pumice bombs were present (to roughly 20 cm) but were not collected due to the need to carry samples down the mountain. Lava flows were also sampled along the headwall's bounding upper west and southeast edges (the latter collected and provided by E. Bard and D. Zimbelman), and from below the unconformity; lava localities that proved suitable for $^{40}Ar/^{39}Ar$ dating are shown in Fig. 3.

2.2. Sunrise Park Road (46.9038° N, 121.5910° W to 46.9052° N, 121.5837° W)

A roughly 2 m thick fall deposit of pumiceous dacite lapilli and coarse ash is exposed intermittently in slope cuts on the north side of the paved road ascending from the White River to Sunrise Park, about 14.5 km east-northeast of Mount Rainier's summit. This site was sampled for U-Th and (U-Th)/He dating of zircon. The pumice at this locality ranges from light brownish white where fresh to yellow where strongly hydrated, the latter accompanied by development of secondary clay at the expense of glass. The five largest lapilli seen at this locality average 6 cm across. Crandell (1969) and Crandell and Miller (1974) noted that the pumice deposit in this area overlies till they assigned to the Hayden Creek Drift and underlies talus that is overlain, in turn, by till they assigned to the Evans Creek Drift. Those and subsequent authors showed that the Evans Creek Drift is a product of the last glacial maximum (marine oxygen isotope stage 2 or MIS 2), whereas the Hayden Creek Drift is the most widespread deposit of alpine glaciers in the region and is mainly a product of the penultimate glaciation (MIS 6). This stratigraphy would bracket the pumice as having been deposited after about 140 ka (Lisiecki and Raymo, 2005) and before the peak of the last glacial maximum at about 27 ka (Clark et al., 2009). These roadcuts are the most accessible sites to examine the pumice directly.

2.3. Baker Point (46.8860° N, 121.6637° W)

Baker Point is a north facing promontory overlooking the head of the White River on the northwest shoulder of Goat Island Mountain about 8 km east-northeast of Mount Rainier's summit. A fall deposit of light brownish white dacite pumice is exposed on the west side of the crest of the ridge about 0.3 km south of the precipice of Baker Point (this exposure is at the north foot of point 6772′ on the USGS Sunrise Quadrangle 1:24,000 topographic map). The pumice deposit is largely concealed by talus blocks but is in the range of 1–3 m thick, and the largest pumiceous pyroclasts are about 7 cm across.

2.4. Burroughs Mountain (46.9095° N, 121.6858° W)

A small (<3 m across) area of light brownish white dacite pumice lapilli (to 7 cm) erodes out from beneath talus on the northeast shoulder of Burroughs Mountain about 8.4 km northeast of Mount Rainier's summit. This exposure is about 0.45 km northeast of the summit of Burroughs Mountain at the brink of its steep north face, 30–40 m above the trail from Sunrise to the summit of Burroughs Mountain. The ground surface across this region is widely blanketed by heterogeneous medium-to-dark brown pumice and scoriae from the Holocene C tephra eruption of Mount Rainier. The small exposure of the dacite of Sunset Amphitheater is distinguished from the C tephra by its uniform light color and conspicuous phenocrysts of amphibole and plagioclase-pyroxene glomeroporphyritic clots. Isolated pumice lapilli of similar size and appearance can also be found on the upper northwest slope of Burroughs Mountain indicating that some dacite of Sunset Amphitheater is preserved in that area within or beneath talus and frost-heaved blocks that mantle the ground surface.

2.5. Ketron Island, Puget Sound (47.1473° N, 122.6392° W)

Bluffs at the south point of Ketron Island, Puget Sound, expose an approximately 10 m thickness of stratified and cross-bedded pumiceous sands containing lenses to 10 cm thick by 20 cm across of white dacite pumice lapilli and small bombs (Walsh et al., 2003a, 2003b). The pumiceous deposit overlies a 5–10 m thickness of pumice-free pebbly sand. The top of the bluff exposes till assigned to the Vashon Drift deposited during or just after the last glacial maximum (MIS 2), but an interval of slope wash separates this from the underlying pumiceous deposit. Based on an early and now known to be erroneous $^{40}Ar/^{39}Ar$ date on plagioclase from the Sunset Amphitheater locality (194 ka), Walsh et al. (2003b) describe this pumiceous sand as having been deposited in MIS 7.

3. Analytical methods

3.1. Whole-rock geochemistry

Major-oxide and trace-element compositions of coarse single pumice pyroclasts (Table 1) were measured by X-ray fluorescence (XRF) and by instrumental neutron activation analysis (INAA) in the laboratories of the USGS in Lakewood, Colorado (Baedecker, 1987), except for samples collected from Ketron Island in 2005 (05KI921-1, 05KI921-2) that were analyzed by XRF and by solution inductively-coupled plasma mass-spectrometry (ICP-MS) at the Washington State University (WSU) GeoAnalytical Laboratory in Pullman, Washington (Johnson et al., 1999; https://environment.wsu.edu/facilities/geoanalytical-lab/technical-notes/icp-ms-method). Whole-rock trace-element concentrations measured by XRF at the USGS were by energy-dispersive methods, whereas those at WSU were by higher precision wavelength-dispersive methods, and the difference in precision is reflected by the reported significant digits in Table 1.

3.2. Glass and mineral compositions

Glass separates were made of two atypically large pumices from the Ketron Island locality and were analyzed by the same XRF and ICPMS methods as their host pumices (Sisson et al., 2014; reproduced in Table 1). Major-oxide compositions of glasses and of representative minerals were also measured in polished thin sections of pumice by wavelength-dispersive methods with the 5-spectrometer JEOL 8900 electron-microprobe at the USGS, Menlo Park, California (Tables 2–5). Background-corrected X-ray count rates were converted to concentrations with the JEOL proprietary version of the CIT-ZAF reduction scheme (Armstrong, 1995) referenced to a variety of natural and synthetic standards. Glasses were analyzed at an accelerating potential of 15 kV, Faraday current of 2 nA, beam diameter of 15–20 μm, with Na-measured first for 5 s, and other elements measured for up to 60 s. These conditions have been shown to reduce the decay of Na count rates in glasses to below detection (Morgan and London, 1996; Ratajeski, 1999). Minerals were analyzed at 15 kV with either a focused (pyroxene, amphibole, FeTi oxides) or 2 μm diameter beam (plagioclase) and a Faraday current of 10 nA. Analyses of FeTi oxides were exclusively of touching titanomagnetite-ilmenohematite pairs within 5 μm of their contacts with glass to assess immediately pre-eruptive T-fO_2 conditions.

3.3. $^{40}Ar/^{39}Ar$ geochronology

$^{40}Ar/^{39}Ar$ age measurements were made on plagioclase phenocryst separates from the Sunset Amphitheater and Ketron Island localities, the latter after HF washing, and on groundmass separates of lavas sampled from the south ridge of Liberty Cap. Ar isotopes were measured with an MAP 216 mass spectrometer by the furnace step-heating approach and ages are reported relative to 28.35 ± 0.01 Ma Taylor Creek sanidine standard (Fleck and Calvert, 2016). Sample processing,

irradiation, monitoring, heating, instrumental analytics, and data reduction are similar to those detailed in Calvert et al. (2005). $^{40}Ar/^{39}Ar$ age measurements were also attempted for amphibole separates from the Sunset Amphitheater and Sunrise Park Road localities but failed to yield interpretable ages due to excess Ar and the abrupt release of nearly all Ar over narrow temperature intervals, and those results are not reported.

3.4. U-Th zircon geochronology

Multiple pumices from the Sunrise Park Road locality were pulverized by hand to <425 μm using a steel plate and cylinder. An aliquant of 114 g was digested in cold concentrated HF over ca. 5 min. The washed acid-insoluble residue was passed through a magnetic separator to remove FeTi oxides and was then separated by density using methylene iodide. Tens of zircon crystals were recovered whose sizes are bimodally distributed: one group has crystals <100 μm at the long axis ("small" or "fine"), whereas the other group has remarkably big crystals that were a few hundreds of microns long ("coarse"). Unpolished small and coarse grains were pressed separately into high purity (6N) indium metal filling holes in a 2.54 cm aluminum disk. The disk was also loaded with pre-polished crystals of AS3 reference zircon from the Duluth Complex (USA) anorthositic series, with a reported U-Pb age of 1099.1 ± 0.2 Ma (Schmitz et al., 2003) which was used as an equilibrium reference; 91500 reference zircon from Kuehl Lake (Canada) syenite was used to estimate U concentrations from measured UO^+/Zr_2O_4 (81 ppm U; Wiedenbeck et al., 1995). Surfaces of zircon in both small and coarse grains were analyzed by SIMS using the University of California Los Angeles (UCLA) CAMECA ims 1270 with a primary beam accelerating voltage of 12.5 kV for an ~50 nA $^{16}O^-$ beam focused into a ~20–40-μm diameter spot (Schmitt, 2011). Positive secondary ions were accelerated at 10 kV and counted by three electron multipliers with respect to mass/charge ratio over total analysis durations of 15 min (small grains) and 90 min (coarse grains). Zirconium oxide ion species were included as reference peaks to center the magnetic field for low-intensity peaks. Backgrounds from tailing of adjacent peaks and potential molecular isobars were subtracted from $^{230}Th^+$ intensities. Relative sensitivity factors were determined from analysis of $^{208}Pb^*/^{206}Pb^*$ (* = radiogenic) on AS3 reference zircon using the method of Reid et al. (1997) and applied to measured atomic $^{238}U^+/^{232}Th^+$ to resolve inter-element fractionation between Th and U. Interspersed analyses of secular equilibrium zircon AS3 yielded U-Th activities (in parentheses) with an average $(^{230}Th)/(^{238}U) = 0.999 \pm 0.016$ (mean square of weighted deviates MSWD = 1.7; number of replicate analyses n = 10) and 0.996 ± 0.034 (MSWD = 0.3; n = 5) for the zircon rim and zircon interior mounts analyzed in two separate analytical sessions (errors 2σ).

Subsequent to the SIMS rim analyses, white light interferometry using a MicroXAM surface profilometer was used to probe sputter pits in every coarse crystal (5 total). For coarse crystals, pits average ~15 μm in depth and the estimated depths for sputter pits in small crystals are ~2.5 μm. After profiling, the coarse grains were extracted, remounted in indium on another mount, and further polished down by ~15 μm until all traces of the pits were removed. Interiors were then analyzed using the same analytical conditions as for the small zircon rim analyses producing ~2.5 μm deep craters.

Bulk tephra $(^{230}Th)/(^{238}U)$ and $(^{230}Th)/(^{232}Th)$ values were used as an anchor for zircon-melt isochrons, assuming that the tephra compositions are representative of the melt from which zircon crystallized (Reid et al., 1997). Small fragments of pumice were analyzed for U and Th isotopic compositions after ion exchange chromatographic purification of U and Th fractions from acid-digested rock powder (Shen et al., 2003) by multi-collector (MC) ICP-MS at National Taiwan University (Shen et al., 2012). Isotope dilution analysis was carried out on a Thermo-Electron Neptune MC-ICP-MS with mass bias corrections and quantification for U abundances based on triple-spike ^{229}Th-^{233}U-^{236}U (Shen et al., 2003, 2012). Age calculations are based on the decay constants recommended by Steiger and Jager (1977) and the ^{230}Th half-life of Cheng et al. (2013).

3.5. (U-Th)/He geochronology

A subset of the small zircon crystals was extracted from the indium metal, photographed, and packed into niobium (Nb) tubes for (U-Th)/He analysis. Procedures followed protocols for noble gas (^4He) and ICP-MS (for U, Th, and Sm abundances) at Curtin University (Danišík et al., 2017). The alpha-ejection correction factor (Ft) was based on optical microscopy to determine crystal dimensions, with corresponding Ft values between 0.73 and 0.86; geometry uncertainties affecting the Ft value are propagated along with the stated total analytical uncertainty. Homogeneous distribution of Th and U is reasonably assumed because SIMS rim and interior analyses of the coarse zircons yielded broadly similar values and no consistent differences between the coarse and fine populations exist (see below). Because no intra- or inter-grain differences were detected for zircon crystallization ages, the error-weighted average age and its uncertainties were used to correct (U-Th)/He ages for the effects of ^{230}Th deficits at the time of eruption which leads to an increase in the (U-Th)/He age relative to the age calculated assuming U-series equilibrium (Farley et al., 2002). Excess ^{231}Pa with initial $D_{Pa/U} = 3$ (Schmitt, 2011) was assumed; because $(^{231}Pa)/(^{235}U)$ at the time of eruption was lower (~1.25), and other short-lived intermediate isotopes are reasonably expected to have been in equilibrium at this time, any uncertainties resulting from disequilibrium corrections besides ^{230}Th are negligible. All corrections were implemented using the MCHeCalc software (Schmitt et al., 2010) which fully propagates individual analytical uncertainties and uncertainties related to the U-Th crystallization age.

4. Mineralogy and geochemistry of the dacite of Sunset Amphitheater

The dacite of Sunset Amphitheater is a porphyritic pumice consisting of 60–65 wt% vesicular rhyolitic glass, about 30 wt% plagioclase, 3–7 wt % pyroxene (augite > hypersthene), 0.5–3 wt% brown amphibole,

Table 2
Major-oxide compositions (wt%) of glasses analyzed by electron-microprobe in pumice thin sections.

Sample	Latitude	Longitude	Locality	n	SiO_2	TiO_2	Al_2O_3	FeO*	MnO	MgO	CaO	Na_2O	K_2O	P_2O_5	Cl	SO_3	Total
93RW96	46.8600	−121.7809	SA	16	74.8	0.30	13.6	1.51	0.02	0.29	1.35	3.96	4.02	0.05	0.15	0.02	94.3
95SR492	46.8862	−121.6625	BP	15	75.0	0.28	13.4	1.46	0.03	0.29	1.34	4.04	3.98	0.03	0.17	0.02	96.1
95WR498	46.9040	−121.5897	SPR	22	75.2	0.24	13.3	1.56	0.05	0.24	1.30	3.90	4.00	0.02	0.16	0.03	96.0
01SR892	46.9095	−121.6858	BM	20	74.8	0.21	13.5	1.48	0.04	0.29	1.36	4.12	4.01	0.03	0.16	0.02	98.2
19-1E-11-73E	47.14717	−122.6377	KI	26	74.1	0.32	13.8	1.79	0.05	0.32	1.50	4.14	3.82	0.05	0.15	0.01	96.2
"	"	"	"	21	74.8	0.30	13.5	1.50	0.06	0.27	1.38	4.02	3.95	0.04	0.14	0.01	94.7
"	"	"	"	15	74.6	0.39	13.6	1.55	0.01	0.33	1.43	4.03	3.94	0.03	0.15	0.01	94.3

Notes: Analyses are normalized to 100% with all Fe as FeO (FeO*); Total gives original analytical sum; n is number of electron-microprobe analyses averaged; locations are NAD27 CONUS latitude and longitude; localities are Sunset Amphitheater - SA, Baker Point - BP, Sunrise Park Road - SPR, Burroughs Mountain - BM, and Ketron Island - KI; values for 19-1E-11-73E are replicates measured in three analytical sessions.

Table 3
Average and extreme major-oxide compositions (wt%) and molar An - Ab - Or of plagioclase phenocrysts analyzed by electron-microprobe in pumice thin sections and in original Ar separate.

Sample	Locality	n	SiO_2	Al_2O_3	FeO*	MgO	CaO	Na_2O	K_2O	BaO	SrO	Total	An	Ab	Or
19-1E-11-74	KI	19	55.7	26.9	0.41	0.03	9.81	5.79	0.33	0.04	0.16	99.1	47.5	50.7	1.9
"	"	max An	54.9	27.1	0.35	0.03	10.33	5.53	0.30	0.04	0.15	98.7	49.9	48.4	1.7
"	"	min An	55.6	26.0	0.42	0.03	9.40	6.08	0.35	0.04	0.19	98.1	45.2	52.8	2.0
93RW96 rims pumice thin sect.	SA	46	57.9	26.7	0.32	0.02	8.64	6.12	0.41	NA	NA	100.1	42.7	54.8	2.4
" "	"	max An	56.8	27.5	0.34	0.03	9.53	5.82	0.36	NA	NA	100.4	46.5	51.4	2.1
" "	"	min An	60.3	25.7	0.24	0.03	6.88	6.88	0.55	NA	NA	100.6	34.4	62.3	3.3
93RW96 Ar separate - lithic?	SA	98	54.5	29.0	0.42	0.08	10.31	5.28	0.31	0.06	NA	100.0	51.0	47.2	1.8
" "	"	max An	47.2	34.2	0.60	0.09	15.90	1.98	0.11	0.04	NA	100.1	81.0	18.3	0.7
" "	"	min An	60.7	24.8	0.28	<0.01	5.74	7.68	0.74	0.05	NA	100.0	28.0	67.7	4.3
95SR492 rims	BP	29	57.5	26.8	0.33	0.03	8.90	6.02	0.39	NA	NA	100.0	43.2	53.8	2.3
" "	"	max An	54.5	28.6	0.37	0.04	11.00	4.85	0.27	NA	NA	99.6	54.8	43.6	1.6
" "	"	min An	59.7	25.3	0.31	0.02	7.23	6.66	0.55	NA	NA	99.8	36.3	60.4	3.3
95WR498 rims	SPR	34	57.9	26.7	0.35	0.03	8.66	6.05	0.42	NA	NA	100.1	43.1	54.4	2.5
" "	"	max An	56.9	27.5	0.32	0.02	9.43	5.46	0.36	NA	NA	100.0	47.8	50.1	2.1
" "	"	min An	58.6	25.9	0.35	0.04	8.07	6.66	0.5	NA	NA	100.1	38.9	58.2	2.9

Notes: n gives number of analyses averaged; NA - not analyzed; max An, min An - single maximum & minimum anorthite measured; FeO* - all Fe as FeO; " - same as entry above.

1–2 wt% FeTi oxides, <0.5 wt% apatite, and traces of zircon and sulfide. The pumice is typically light brownish white but alters to yellowish brown in localities persistently saturated with water. The glass is colorless and highly inflated with spherical vesicles, and it includes sparse microphenocrysts, but it lacks acicular or skeletal microlites. Glass major-oxide compositions differ little between analyzed samples and are homogenous or nearly so (Table 2). Quenched magmatic inclusions (enclaves) of more mafic material, indicative of magma mingling (Bacon, 1986), have not been recognized in any of the exposures of the dacite of Sunset Amphitheater.

Plagioclase forms tabular phenocrysts with maximum lateral dimensions of 2 × 1 mm, but more commonly are 1.5–0.5 × 0.6–0.3 mm and range down to sparse microphenocrysts as small as ~30 × 15 μm. Although most plagioclase phenocrysts are tabular, their surfaces against glass range from idiomorphic, through slightly scalloped or rounded, to cellular, consistent with diverse histories of growth or weak resorption approaching the time of eruption. Small inclusions of other minerals and of colorless glass are widespread but not abundant, the latter mainly appearing sealed as opposed to interconnected or "spongy". The outer 50–150 μm of the more idiomorphic phenocrysts are weakly normally zoned with compositions in the range An_{55}-An_{34}, averaging about An_{43} (Table 3).

Shiny, dark brown phenocrysts of amphibole are eye-catching in hand samples and thin sections but, although conspicuous, are not abundant (≤3 wt%). Amphibole phenocrysts range in size up to 1.5 × 1 mm, but are more typically 1–0.3 × 0.5–0.15 mm. The phenocrysts are blocky with several (or all) planar, idiomorphic faces against glass, but it is common for at least one grain face to be irregular, consistent with breakage before or during eruption. Completely lacking are degassing-driven breakdown rims of opaque oxides, pyroxene, plagioclase, and melt ("opacite"), consistent with rapid eruptive ascent from depths at which amphibole was stable. The few amphiboles analyzed (Table 4) have compositions similar to those of medium-Al amphibole phenocrysts from Mount St. Helens (Thornber et al., 2008) except for having slightly higher concentrations of K_2O, a difference that also distinguishes rocks and glasses from the two volcanoes (Sisson et al., 2014; Walsh et al., 2003b). Amphibole phenocrysts contain minor inclusions mainly of FeTi oxides and apatite. Melt inclusions are rare, and the amphiboles lack obvious evidence of resorption either on grain surfaces or as internal resorption-overgrowth boundaries.

Phenocrysts to microphenocrysts of augite and hypersthene are more abundant (3–7 wt%) than amphibole (≤3 wt%) but are less obvious due to their smaller sizes (from 0.75 × 0.3 mm down to 30 × 15 μm), paler colors, and duller lusters. Most pyroxene phenocrysts are euhedral against glass with blocky shapes and prominent cleavage. Inclusions of FeTi oxides and of tiny apatites are widespread, the latter often aligned parallel to grain faces. Colorless glass inclusions are present, although not abundant, and as in plagioclase appear mainly to be discrete and contained, rather than interconnected. Augite appears to be much more abundant than hypersthene, judging from birefringence and extinction angles, but their relative proportions have not been measured.

Ilmenohematite and titanomagnetite are widespread both as microphenocrysts and as inclusions, particularly in pyroxenes. Compositions of touching idiomorphic pairs adjacent to glass in pumices from the Sunset Amphitheater and Baker Point localities give temperatures of 860–875 °C and fO_2 0.9–1.0 $\log_{10}$ units greater than the Ni-NiO buffer (Ghiorso and Evans, 2008); a pumice from Ketron Island gives slightly cooler temperatures of 844–860 °C and less oxidized fO_2 of 0.7–0.9 $\log_{10}$ units greater than Ni-NiO (Table 5). Zircon saturation temperatures (Harrison and Watson, 1983) calculated for glasses separated from Ketron Island pumice are similar but slightly cooler, in the vicinity of 815 °C, but this difference is not meaningful considering the accuracy of the methods. Sparse, minute blebs of Fe-Cu sulfide are easily seen under reflected light from their golden yellow color as inclusions in FeTi oxide microphenocrysts. Where the sulfide contacts external glass, it has broken down to a granular, non-reflective material rich in iron oxide. Apatite and zircon also form sparse, tiny inclusions in FeTi oxides.

In addition to phenocrysts, nearly every thin section of pumice intersects from one to a few poly-granular aggregates of plagioclase accompanied by sub-equal amounts of pyroxene, amphibole, or both, as well as by opaque oxide, and in some, glass. These "glomeroporphyritic clots" can be up to about 4 mm across, and their constituent mineral grains are similar in size and habit to many free phenocrysts in the pumice. Differences are that in glomeroporphyritic clots that contain both amphibole and augite, the amphibole partly encases resorbed augite,

Table 4
Average major-oxide compositions (wt%) of mafic phenocryst rims analyzed by electron-microprobe in pumice thin sections.

Sample	Locality	n	Mineral	SiO_2	TiO_2	Al_2O_3	FeO*	MnO	Cr_2O_3	MgO	CaO	Na_2O	K_2O	BaO	Total
19-1E-11-73	KI	11	opx	52.5	0.13	0.55	21.5	0.65	0.01	22.3	0.96	0.01	0.00	0.00	98.6
"	"	15	cpx	51.7	0.30	1.44	9.34	0.32	0.00	14.0	20.8	0.38	0.00	0.00	98.3
"	"	8	amph	42.9	2.72	10.8	12.9	0.21	0.03	13.4	10.7	2.41	0.44	0.06	96.6

Notes: n gives number of analyses averaged; orthopyroxene - opx, clinopyroxene - cpx, amphibole - amph; all Fe reported as FeO (FeO*); " - same as entry above.

Table 5
Average major-oxide compositions (wt%), and T and fO_2, from rims of touching magnetite-ilmenite pairs in pumice thin sections.

Sample	Locality	n	SiO_2	TiO_2	Al_2O_3	FeO*	MnO	MgO	NiO	V_2O_3	Cr_2O_3	T °C	Δ NNO
93RW96													
ilm 1	SA	2	0.03	42.58	0.24	50.79	0.41	2.81	0.01	0.24	0.03	870	0.86
tmt 1	SA	3	0.06	9.13	2.10	80.67	0.29	1.72	0.02	0.58	0.25		
ilm 2	SA	2	0.04	42.08	0.22	51.44	0.40	2.85	0.00	0.20	0.03	861	0.96
tmt 2	SA	3	0.08	8.58	2.13	81.13	0.32	1.77	0.03	0.51	0.18		
ilm 3	SA	3	0.03	42.18	0.23	51.83	0.39	2.85	0.03	0.25	0.06	870	0.95
tmt 3	SA	4	0.06	8.79	2.06	80.82	0.32	1.77	0.03	0.59	0.24		
ilm 4	SA	3	0.02	42.45	0.22	51.28	0.41	2.78	0.02	0.28	0.04	875	0.88
tmt 4	SA	3	0.07	9.18	2.06	80.66	0.31	1.74	0.03	0.58	0.25		
95SR492													
ilm 1	BP	5	0.03	41.65	0.22	51.25	0.36	2.90	0.02	0.24	0.04	870	0.96
tmt 1	BP	5	0.06	8.70	2.01	80.58	0.31	1.77	0.01	0.63	0.24		
ilm 2	BP	4	0.02	41.76	0.22	51.26	0.41	2.86	0.01	0.23	0.04	869	0.95
tmt 2	BP	4	0.07	8.71	2.06	80.67	0.32	1.75	0.04	0.58	0.23		
ilm 3	BP	3	0.02	41.49	0.23	51.01	0.44	2.90	0.02	0.27	0.03	872	0.96
tmt 3	BP	3	0.09	8.78	2.03	80.42	0.31	1.82	0.03	0.59	0.21		
ilm 4	BP	4	0.02	42.36	0.23	51.09	0.40	2.83	0.02	0.23	0.04	867	0.94
tmt 4	BP	3	0.08	8.91	2.09	79.72	0.33	1.77	0.02	0.59	0.29		
19-1E-11-73E													
ilm 1	KI	15	0.09	42.87	0.25	51.30	0.42	2.81	0.01	0.21	0.05	860	0.91
tmt 1	KI	15	0.09	9.10	2.08	82.27	0.33	1.71	0.03	0.61	0.21		
ilm 2	KI	5	0.04	44.30	0.24	49.56	0.41	2.72	0.01	0.21	0.05	844	0.67
tmt 2	KI	10	0.18	8.91	2.07	77.66	0.35	1.72	0.01	0.61	0.28		
ilm 3	KI	10	0.07	43.12	0.24	48.71	0.41	2.87	0.01	0.24	0.03	860	0.70
tmt 3	KI	5	0.07	9.31	2.08	77.75	0.35	1.89	0.02	0.58	0.14		
ilm 4	KI	3	0.04	42.73	0.25	48.04	0.41	2.95	0.04	0.17	0.02	852	0.70
tmt 4	KI	2	0.14	9.23	2.07	79.80	0.39	1.84	0.09	0.53	0.14		

Notes: associated pairs designated by suffix number; n gives number of analyses averaged; FeO* is all Fe as FeO; T and fO_2 from Ghiorso and Evans (2008) with fO_2 reported as deviation in $\log_{10}$bars from O'Neill and Pownceby (1993) Ni-NiO oxygen buffer.

whereas the two minerals are unassociated as phenocrysts. Symplectites of opaque oxide are also present in pyroxene in some glomeroporphyritic clots, albeit rarely. In other Mount Rainier volcanic rocks such oxide-pyroxene symplectites can be seen to be reaction products between melt and olivine that produced pyroxene and Fe-oxide, although olivine has not been found in the dacite of Sunset Amphitheater. Nakada et al. (1994) interpret that similar glomeroporphyritic clots in rhyodacite lava flows of Mount Mazama, Oregon, formed as crystal segregations on the margins of magma conduits and reservoirs that were then re-entrained and variably disaggregated to provide most of the phenocrysts in those lavas. Disaggregation of largely solidified material is a plausible interpretation for those phenocrysts in the dacite of Sunset Amphitheater that lack idiomorphic margins, although the near-constant bulk compositions of the pumices (Table 1) would require that entrainment and disaggregation were minor, that the entrained materials were dispersed uniformly, or that the magma and entrained bulk solid did not differ appreciably in composition.

Zircon crystals in the dacite of Sunset Amphitheater are euhedral, but their tips and edges are often slightly rounded, and crystals contain abundant inclusions (glass, apatite, opaques). The presence of zircon crystals unusually coarse for volcanic rocks, as well as slight rounding, suggest that those zircon crystals may have been liberated by disintegration of a highly solidified part of the magmatic system and incorporated into the magma that erupted as the dacite of Sunset Amphitheater.

5. Attempts to date the eruption of the dacite of Sunset Amphitheater

5.1. Erroneous $^{40}Ar/^{39}Ar$ date from Sunset Amphitheater

The first attempt to date the deposit was made on plagioclase separated from sample 93RW96, which is a 3.8 l (gallon) bag of tephra, mainly coarse pumice lapilli, shed from the pumice band in Sunset Amphitheater. This initial experiment (98Z0286) was overseen by M.A. Lanphere, USGS, who derived a preferred plateau age of 194 ± 25 ka (2σ, 77% ^{39}Ar in plateau, 750–1200 °C) and an isochron age of 185 ± 108 ka (2σ) referenced to an age for the Taylor Creek Rhyolite sanidine of 27.92 Ma. These isochron and plateau ages were reported in Walsh et al. (2003b) and were used in John et al. (2008). Isotopic measurements for this experiment were reexamined prompted by the later production of much younger $^{40}Ar/^{39}Ar$ plagioclase ages for the Ketron Island locality. Re-reduction of the measurements and adoption of a new standard age of 28.35 ± 0.01 Ma for Taylor Creek sanidine (Fleck and Calvert, 2016) yields a plateau age of 206 ± 31 ka (2σ, 65% ^{39}Ar in plateau, 850–1200 °C, MSWD 1.31) and an isochron age of 171 ± 81 ka (2σ, MSWD 1.34) (Table 6; Fig. 4). Two additional age measurements were then attempted on splits of the original plagioclase separate, one of which (experiment 18Z0173) yielded plateau and isochron ages of 215 ± 35 ka (2σ, 78% ^{39}Ar in plateau, 600–1100 °C, MSWD 0.48) and 196 ± 63 ka (2σ, MSWD 0.48) in agreement with the original result, and the other of which (experiment 18Z0172) failed to yield an interpretable age due to scatter. The two plateau ages, although in agreement and acceptably precise, are inconsistent with the stratigraphic relations at the Sunrise Park Road locality, and if that age were that of the pumice eruption, would either invalidate assignment of the underlying till to the Hayden Creek Drift or would invalidate the correlation of the various pumice exposures despite their multiple similarities.

A distinctly low K/Ca ratio is derived from all the Ar isotopic experiments on the original plagioclase separate which is distinct from higher K/Ca ratios derived for plagioclase from pumice collected at Ketron Island and measured directly by electron microprobe in plagioclase phenocrysts in thin sections of pumice from all localities, including from Sunset Amphitheater sample 93RW96. This disparity in composition was confirmed by electron microprobe analysis in the present study, with a grain mount of the original mineral separate yielding average K/Ca (molar) of 0.036 (98 random points) versus 0.048 (77 random points) for plagioclase in a thin section of the 93RW96 pumice analyzed in the same session (K/Ca of plagioclase phenocryst rims are generally even higher: Table 3). Notably, that examination further revealed that grain surfaces in the separate are naturally etched and pitted, with surfaces and etch pits variably coated and filled with Ca- and F-rich clay,

and revealed the presence of sparse grains of calcite. These hydrothermal alteration features are absent from plagioclase in all thin sections of pumice lapilli from all localities of the dacite of Sunset Amphitheater, including Sunset Amphitheater itself, which points to the original plagioclase separate having been made of material other than the intended fresh pumice. Lava flows with eruption ages near 200 ka are exposed close to Sunset Amphitheater, and the plagioclase separate may have been prepared from lava lithics within the 93RW96 sample, possibly as extraneous material frozen to the surfaces of the pumice lapilli when collected, and then shed upon warming. The reproducible $^{40}Ar/^{39}Ar$ plateau age slightly >200 ka may date the eruption of the lava from which the lithic debris originated, but it is abandoned as the eruption age of the dacite of Sunset Amphitheater.

5.2. $^{40}Ar/^{39}Ar$ on plagioclase from Ketron Island

A Pleistocene pumiceous deposit exposed at the south end of Ketron Island, southern Puget Sound (T. Walsh, personal communication) was sampled by boat access. Whole-rock, glass, and mineral compositions, as well as mineral assemblage of pumice from Ketron Island proved to be similar to those of the dacite of Sunset Amphitheater on and close to Mount Rainier, supporting their correlation (Tables 1–5). Age measurements were made by the $^{40}Ar/^{39}Ar$ method on a coarser grained (250–425 μm) and a finer grained (106–250 μm) split of HF-treated plagioclase phenocrysts separated by crushing from Ketron Island sample 05KI921. The coarser split yielded a plateau age of 138 ± 20 ka (2σ, 68% ^{39}Ar in plateau, 725–1100 °C, MSWD 1.23) and an isochron age of 134 ± 36 ka (2σ, MSWD 1.49), whereas the finer split gave a plateau age of 101 ± 11 ka (2σ, 55% ^{39}Ar in plateau, 800–1025 °C, MSWD 0.50) and an isochron age of 94 ± 32 ka (2σ, MSWD 0.62) (Table 6; Fig. 4). Ages from either split are consistent with eruption between the penultimate glaciation and the last glacial maximum as interpreted by Crandell and Miller (1974) for the exposures along the Sunrise Park Road. The consistency between the plateau and isochron results for each split might individually be taken as indicating a robust result, but the plateau ages of the two splits fail to overlap at the 2σ level.

5.3. U-Th on zircon from Sunrise Park Road

The apparent 100 kyr spread of $^{40}Ar/^{39}Ar$ age results (before discovery of the probable non-pumice origin of the ~200 ka plagioclase) prompted alternative efforts to date the pumice deposit. Zircon crystals were separated from a composite sample of pumice lapilli from the Sunrise Park Road locality, divided into finer (<100 μm at the long axis) and coarser fractions, and dated by the U-Th disequilibrium method by SIMS at the University of California, Los Angeles (Table 7). Zircon rims have U abundances of 89–543 ppm (average: 188 ppm), similar to zircon interiors with 85–210 ppm (average: 138 ppm). Analyses of individual pumice pyroclasts yield average U concentrations of 4.11 ± 0.68 ppm (2σ), and glass separated from two pumice bombs from the Ketron Island locality have U concentrations averaging 6.465 ± 0.014 ppm (Table 1). These concentrations would indicate average zircon-melt partitioning coefficients D_U of ~30–45, at the lower limit of values measured for rhyolitic melts (Wright et al., 2015; Blundy and Wood, 2003), but in the range produced experimentally for zircon grown from H_2O-rich dacitic to rhyolitic melts (Rubatto and Hermann, 2007). $(^{238}U)/(^{232}Th)$ in zircon rims and interiors average 5.6 and 5.1, respectively, with ranges from 4.5–7.8 (rims) to 4.2–6.6 (interiors). Pumice pyroclasts and glass separates have average $(^{238}U)/(^{232}Th)$ calculated as 1.10 and 1.07, respectively, (from Table 1), whereas $(^{238}U)/(^{232}Th)$ measured by isotope dilution mass spectrometry on two small splits of pumice averages 0.928 (Table 7), possibly indicating minor U-loss by recent weathering of fine glass. These activity ratios correspond to $D_{Th/U} = 0.17–0.22$, similar to the $D_{Th/U} = 0.15–0.19$ for natural rhyolite glass – zircon-rim pairs (Wright et al., 2015; Blundy and Wood, 2003), but lower than experimental $D_{Th/U} = 0.25–0.41$ for H_2O-rich dacitic and rhyolitic melts (Rubatto and Hermann, 2007). The consistency of zircon-melt apparent partitioning for Th and U supports that whole-rock concentrations and activity ratios are acceptable proxies for the melt from which zircon crystallized. Zircon values plot strongly to the right of the equiline on the $(^{230}Th)/(^{232}Th)$ versus $(^{238}U)/(^{232}Th)$ diagram (Fig. 5), due to the preference of zircon for U relative to Th. The pumice or melt values are close to or on the equiline, showing either a slight excess in ^{230}Th with $(^{230}Th)/(^{238}U) = 1.12 \pm 0.01$ using the mass-spectrometric measurements of composite pumice fragments (Table 7), or a slight ^{230}Th deficiency with $(^{230}Th)/(^{238}U) = 0.97 \pm 0.01$ combining mass-spectrometric $(^{230}Th)/(^{238}U)$ with $(^{238}U)/(^{232}Th)$ derived from the glass-separate Th and U concentrations (Table 1; all errors 2σ). A published U-series datum for Mount Rainier also shows a slight ^{230}Th excess (andesite RV-6 in Newman et al., 1986) (Figs. 5 and 6).

Regression of the zircon results requiring that the regression passes through the bulk ash $(^{238}U)/(^{232}Th)$ and $(^{230}Th)/(^{232}Th)$ (Table 7) yields

Table 6
$^{40}Ar/^{39}Ar$ results.

Sample	Locality	Latitude	Longitude	Material	$^{40}Ar/^{39}Ar$ weighted mean plateau age			$^{40}Ar/^{39}Ar$ isotope correlation (isochron) age				$^{40}Ar/^{39}Ar$ total gas
					Age (ka)	%^{39}Ar[steps, °C]	MSWD	Age (ka)	%^{39}Ar[steps, °C]	MSWD	$^{40}Ar/^{36}Ar_i$	Age (ka)
93RW96 - lithic?	SA	46.8600	−121.7809	Altered plag	205.6 ± 30.7	65 [850–1200]	1.31	170.9 ± 80.5	65 [850–1200]	1.34	301.4 ± 14.1	347.8 ± 3.4
93RW96 - lithic?	SA	46.8600	−121.7809	Altered plag	214.6 ± 28.2	78 [600–1100]	0.48	195.8 ± 74.3	78 [600–1100]	0.48	303.0 ± 15.6	393.6 ± 41.4
05KI921-coarse	KI	47.1472	−122.6377	Pumice plag	138.0 ± 19.7	68 [725–1100]	1.23	134.4 ± 36.1	68 [725–1100]	1.49	299.0 ± 3.7	175.3 ± 11.8
05KI921-fine	KI	47.1472	−122.6377	Pumice plag	100.5 ± 10.9	55 [800–1025]	0.50	94.2 ± 32.4	55 [800–1025]	0.62	300.8 ± 10.5	122.6 ± 9.6
94RW357	SA SE edge 4100 m	46.8599	−121.7734	Lava gm	90.9 ± 10.2	93 [625–1100]	0.76	88.3 ± 20.7	93 [625–1100]	0.87	299.0 ± 2.8	95.3 ± 11.0
94RW359	SA SE edge 4220 m	46.8612	−121.7738	Lava gm	54.4 ± 4.2	94 [700–1200]	0.20	55.2 ± 8.5	94 [700–1200]	0.22	298.1 ± 4.4	55.8 ± 5.0

Notes:
Flux monitor: 28.345 Ma Taylor Creek sanidine.
Atmospheric argon: 298.56 ± 0.31.
All errors ±95% confidence.
plag - plagioclase, gm - groundmass.
SA - Sunset Amphitheater.
Latitude and longitude are NAD27 CONUS.

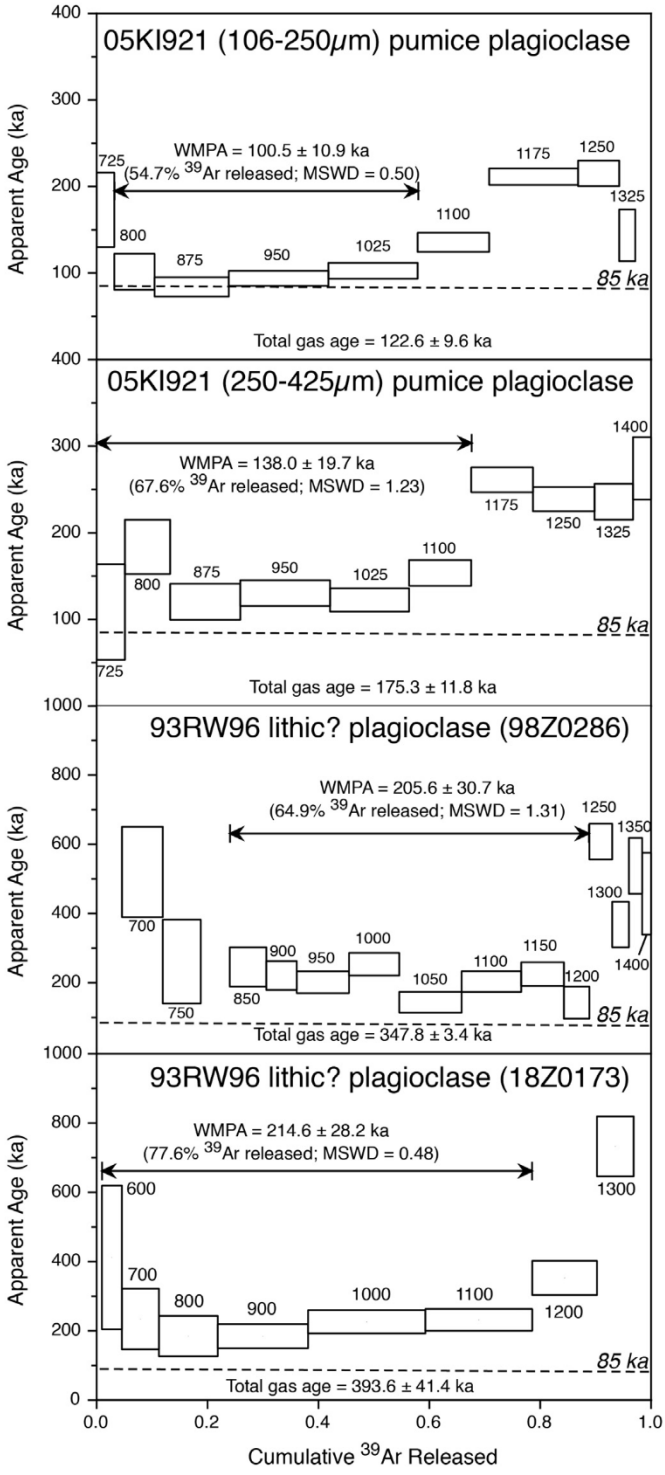

Fig. 4. $^{40}Ar/^{39}Ar$ age spectra for plagioclase separated from pumice exposed at Ketron Island (05KI921) and from probable lithic debris within bulk pumiceous tephra from Sunset Amphitheater (93RW96). Brackets on age spectra show heating steps that yield statistically permissible weighted mean plateau ages (WMPA). Dashed line shows the best-fit 85 ka eruption age determined by (U-Th)/He on zircon. Uncertainty brackets on heating steps are ±1σ.

an average zircon rim model age (including coarse and fine grains) of 147 ± 8 ka (MSWD = 1.12; n = 28; 2σ error), which is indistinguishable from the average zircon interior age of 148 ± 36 ka (MSWD = 0.83; n = 5). Combining rim and interior ages yields an average model age of 147 ± 8 ka (MSWD = 1.01; n = 33). MSWD values near unity are consistent with a uniform U-Th age population. Inconsequential age differences result if the melt end-member of the isochron is instead derived by combining mass-spectrometric (^{230}Th)/(^{238}U) with concentration-derived (^{238}U)/(^{232}Th) from glass (Table 1). These zircon-melt model ages are older than model ages derived by regressing the zircon U-Th results without requiring passing through the pumice (^{238}U)/(^{232}Th) and (^{230}Th)/(^{232}Th). Data-defined regression of the U-Th results yields an age of 109 ± 68 ka (MSWD 1.01; n = 23) for the small zircon rims and of 100 ± 36 ka (MSWD 1.09; n = 10) for coarse zircon (rims and interiors). Using the data-defined U-Th isochron age could be justified if zircon crystallized from more evolved melts than measured in the bulk pumice. However, the unusually high values for (^{230}Th)/(^{232}Th) and (^{238}U)/(^{232}Th) of ~2.73 obtained from the intercept of the zircon-only regression with the equiline greatly exceed those observed for Quaternary Cascade volcanic rocks and glasses (Newman et al., 1986; Reagan et al., 2003; Jicha et al., 2009; Ankney et al., 2013), which argues against the reliability of the zircon-only regression age, although it yields a statistically valid regression.

5.4. (U-Th)/He on zircon from Sunrise Park Road

Sunset Amphitheater (U-Th)/He zircon ages were obtained for 16 zircon crystals from the Sunrise Park Road locality (Table 8). These are "fine" grains that were previously dated by U-Th methods; "fine" grains were employed because they had not been subjected to a polishing step and therefore retained their original symmetric shapes allowing for simpler and more reliable characterization of grain geometry. Without correction for disequilibrium, the average (U-Th)/He age would be ca. 70 ka, but because of the effects of U-series disequilibrium, this minimum "equilibrium" age significantly underestimates the true age (Farley et al., 2002). A maximum model age is derived by assuming instantaneous eruption after zircon crystallization (i.e. "complete disequilibrium"). For the Sunset Amphitheater zircon population, the complete disequilibrium age averages ca. 105 ka. Because zircon may have crystallized closer to 147 ka, based on U-Th disequilibrium dating, and therefore would have experienced significant pre-eruptive crystal residence, the complete-disequilibrium age overestimates the true eruption age. Therefore, both factors, initial disequilibrium and pre-eruptive crystal residence, are accounted for in the "disequilibrium-corrected" age of 85 ± 6 ka (95% confidence; MSWD = 4.7; n = 16; Fig. 6). The stated uncertainty of the disequilibrium-corrected age was estimated from the error for the average age, weighted for analytical uncertainties of the individual measurements, and accounting for excess scatter by multiplying that uncertainty by the square-root of the MSWD. This protocol acknowledges that there are unpropagated analytical uncertainties in (U-Th)/He zircon geochronology, for example, those relating to compositional or age zonation of the analyzed crystals (Danišík et al., 2017). For zircon crystallization at ca. 106 ka (data-defined isochron age combining all zircons), the resulting disequilibrium-corrected age would be close to the complete-disequilibrium age. We interpret the comparatively large overall sizes of the zircon crystals (coarse and fine) as possibly due to derivation of those grains from a largely crystalline source. If so, the older U-Th crystallization ages may be closer estimates of when most zircon grew, and the 85 ± 6 ka (2σ) (U-Th)/ He zircon date would be the best estimate for the eruption of the dacite of Sunset Amphitheater.

5.5. $^{40}Ar/^{39}Ar$ ages of lava flows along the margin of Sunset Amphitheater

Lava flows high on Mount Rainier tend to be partially glassy, fine-grained, and porous, making them poor candidates for $^{40}Ar/^{39}Ar$ dating. Two lava samples collected from the south ridge of Liberty Cap along the southeast margin of Sunset Amphitheater Headwall (Fig. 3), nevertheless have sufficiently dense and coarsely crystallized groundmasses to date by the $^{40}Ar/^{39}Ar$ chronometer (Table 6). The stratigraphically lower sample, 94RW357 from 4100 m elevation, yields Ar plateau and isochron ages of 90.9 ± 10.2 ka (2σ, 93% ^{39}Ar in plateau, 625–1150 °C,

Table 7
SIMS U-Th zircon results for composite pumice sample from Sunrise Park Road.

Material	(^{238}U)/(^{232}Th)	±(1sd)	(^{230}Th)/(^{232}Th)	±(1sd)	m	±(1sd)	Age (ka)	+(1sd)	−(1sd)	U (ppm)
Core coarse 1	4.15	0.05	3.62	0.24	0.800	0.074	175	51	−34	177
Core coarse 2	6.21	0.09	4.21	0.68	0.599	0.130	99.9	42.8	−30.7	111
Core coarse 3	6.57	0.08	4.60	0.61	0.632	0.109	109	38	−28	85
Core coarse 4	4.21	0.05	3.54	0.23	0.760	0.071	156	38	−28	210
Core coarse 5	4.53	0.06	4.05	0.52	0.835	0.145	197	230	−69	106
Rim coarse 1	5.38	0.05	4.34	0.12	0.742	0.029	148	13	−11	120
Rim coarse 2	5.86	0.06	4.49	0.12	0.699	0.027	131	10	−9	126
Rim coarse 3	6.71	0.07	5.21	0.16	0.720	0.028	139	12	−11	113
Rim coarse 4	7.82	0.08	5.85	0.23	0.698	0.034	131	13	−12	89
Rim coarse 5	4.66	0.04	3.91	0.09	0.770	0.024	160	12	−11	134
Rim small 1	5.27	0.06	5.07	0.33	0.929	0.078	289	∞	−80	167
Rim small 2	4.72	0.12	3.66	0.26	0.692	0.071	128	29	−23	206
Rim small 3	4.94	0.06	4.06	0.23	0.751	0.059	152	30	−23	254
Rim small 4	6.99	0.06	5.85	0.50	0.793	0.083	172	56	−37	118
Rim small 5	4.69	0.04	3.80	0.30	0.733	0.080	144	39	−29	120
Rim small 6	4.99	0.04	4.34	0.33	0.814	0.083	184	64	−40	225
Rim small 7	4.67	0.05	3.97	0.32	0.783	0.086	167	55	−36	152
Rim small 8	5.21	0.04	4.70	0.32	0.854	0.075	210	79	−45	159
Rim small 9	4.98	0.16	4.65	0.41	0.891	0.106	242	381	−74	173
Rim small 10	5.79	0.09	4.60	0.43	0.733	0.089	144	44	−31	164
Rim small 11	5.70	0.12	4.90	0.36	0.810	0.078	182	58	−38	183
Rim small 12	5.30	0.04	4.58	0.30	0.811	0.070	182	50	−34	248
Rim small 13	5.39	0.05	4.19	0.24	0.707	0.055	134	23	−19	244
Rim small 14	4.55	0.05	3.74	0.31	0.745	0.086	149	45	−32	136
Rim small 15	4.56	0.05	3.93	0.28	0.793	0.079	172	53	−35	308
Rim small 16	5.87	0.08	4.33	0.27	0.666	0.056	120	20	−17	201
Rim small 17	6.06	0.07	5.11	0.42	0.793	0.083	172	56	−37	163
Rim small 18	6.35	0.07	4.51	0.50	0.639	0.093	111	32	−25	101
Rim small 19	5.47	0.05	4.64	0.24	0.793	0.053	172	32	−25	543
Rim small 20	5.99	0.05	4.71	0.32	0.725	0.063	141	28	−22	301
Rim small 21	7.80	0.07	6.31	0.78	0.767	0.114	159	73	−44	98
Rim small 22	5.11	0.04	4.56	0.32	0.842	0.077	202	73	−43	188
Rim small 23	5.87	0.12	4.16	0.25	0.631	0.053	109	17	−15	239

Notes: sample collected at latitude 46.9036, longitude −121.5908; m = isochron slope for zircon and melt (from whole-rock composition measured by isotope dilution multi-collector ICP-MS); whole-rock compositions are average from two aliquots: (^{238}U)/(^{232}Th) = 0.928 ± 0.003; (^{230}Th)/(^{232}Th) = 1.040 ± 0.005; (^{234}U)/(^{238}U) = 1.002 ± 0.002 (aliquot 2 only).

MSWD = 0.76) and 88.3 ± 20.7 ka (MSWD = 0.87) (Table 6). Although the dacite of Sunset Amphitheater was not seen along the visited east side of the ridge crest, this lava sample was collected at or shortly higher than where the deposit's apparent dip would project to the ridge. The age represents that of lava that erupted close to or shortly after the pumice. The higher sample, 94RW359 from 4220 m elevation, was collected appreciably above the pumice stratigraphically. Its Ar plateau and isochron ages are 54.4 ± 4.2 ka (2σ, 94% ^{39}Ar in plateau, 700–1200 °C, MSWD = 0.2) and 55.2 ± 8.5 ka (MSWD = 0.22).

6. Discussion

The robust result for the dacite of Sunset Amphitheater suggests eruption between ca. 91 and 78 ka based on the 95% confidence range of the (U-Th)/He age. This is consistent with the ^{40}Ar/^{39}Ar plateau and isochron ages determined for groundmass of lava at about the equivalent stratigraphic position along the southeast rim of Sunset Amphitheater Headwall (Fig. 3), and it overlaps within 2σ uncertainty with the ^{40}Ar/^{39}Ar plateau and isochron ages for the fine plagioclase split from Ketron Island pumice. Zircon U-Th model ages are generally older, as are the apparent ^{40}Ar/^{39}Ar ages for Ketron Island coarse plagioclase (Fig. 7). As noted, the published ~200 ka age for the dacite of Sunset Amphitheater results from a sample preparation error, does not date the pumice eruption, and is excluded from further consideration. That zircon U-Th and U-Pb ages can record growth prior to eruption is known from many studies (e.g., Schmitt, 2011, and references therein). Zircon U-Th model ages for the dacite of Sunset Amphitheater differ if their isochrons are or are not required to pass through the bulk tephra, although the older tephra-constrained age avoids an atypically high equiline intercept and is preferred. Mount Rainier's edifice commenced growth at close to 500 ka atop the deeply incised remains of an ancestral volcano that was chiefly active ≥1 Ma, and its subsequent history falls into four alternating periods of rapid and modest effusion each on the order of 80–180 kyr duration. The last period of high effusion ended gradually around 150–160 ka (Sisson et al., 2001), and it is possible that the pumice-constrained average U-Th zircon model age of 147 ± 8 ka records solidification beneath the volcano during that time of waning magmatic flux. A later magmatic event may then have partly remelted that domain, leading to segregation and explosive eruption of the dacite. If this interpretation is correct, it would indicate that the dacite magma and zircon therein remained a closed system, or nearly so, with respect to U, Th, and their isotopes from the time of zircon growth through remobilization and eruption 50–70 kyrs later. On the other hand, the volcano remained active over that age period, and continuous zircon growth may have occurred during various cooling and solidification events closer to the time of the final explosive eruption. Resolving between these interpretations would require additional and higher-precision U-Th isotopic results.

6.1. Undegassed melt inclusions as the cause of erroneously old ^{40}Ar/^{39}Ar apparent ages

The erroneously old apparent age for the coarse split of plagioclase from Ketron Island is a cautionary lesson on the requirements of successful ^{40}Ar/^{39}Ar dating. That method is predicated on a sample being dominated by two Ar sources, one being the ^{40}Ar grown by decay of ^{40}K since cooling below the closure temperature, and the other being trapped Ar that in a step-heating experiment can be identified as having ^{39}Ar/^{40}Ar of zero (no ^{39}Ar produced in the reactor from ^{39}K). Routinely, this trapped component has the isotopic composition of air. Individual heating steps measure composites of these two endmembers. Real samples may, however, contain a third (or more) sources of Ar generally referred to as "excess" that typically are enriched in ^{40}Ar (Dalrymple and Moore, 1968; Kelley, 2002). So long as the abundances of the excess ^{40}Ar

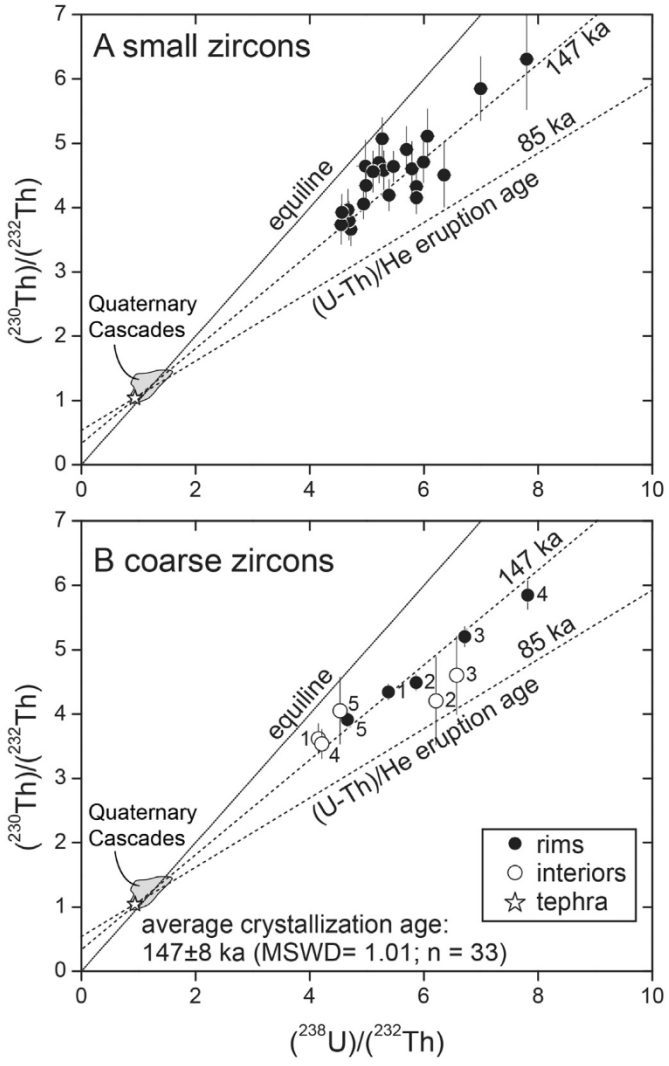

Fig. 5. U-Th isotope plots for fine and coarse zircons (circles) and bulk tephra (star) from the Sunrise Park Road locality. Dashed line labeled 147 ka shows the best-fit U-Th crystallization age for zircon estimated by requiring the (^{238}U)/(^{232}Th) vs. (^{230}Th)/(^{232}Th) regression to pass through the tephra. Shown for reference are an 84.7 ka isochron matching the best-fit U-Th/He age for the eruption, and a zero-age isochron, both also required to pass through the bulk pumice. Shaded field near the origin shows Th-U isotopic values for Quaternary volcanic rocks and glasses from the Cascades magmatic arc after compilations in Jicha et al. (2009) and Ankney et al. (2013).

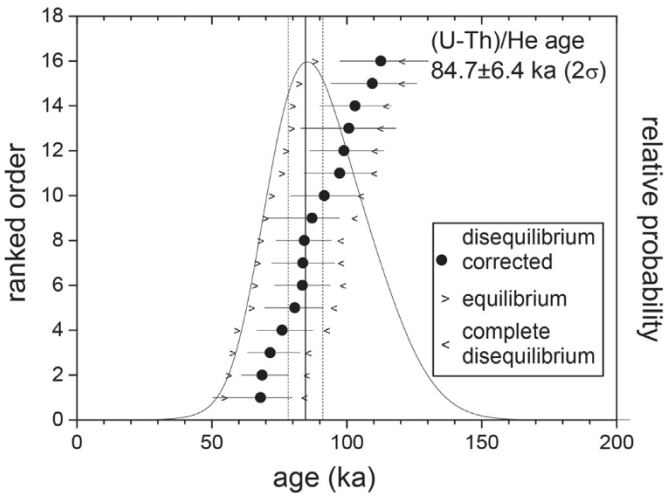

Fig. 6. (U-Th)/He results for individual zircon and derived probability density function for the Sunrise Park Road locality. Probability density function and best-fit age and age uncertainty are derived for the disequilibrium corrected age results (circles). Limiting minimum (>) and maximum (<) ages are shown assuming U-Th isotopic equilibrium and complete disequilibrium, respectively.

components are low relative to the radiogenic ^{40}Ar, the age measurement can still be successful, but for young, low-K samples this can break down.

Step-heating results for the two Ar experiments on Ketron Island plagioclase are shown in Fig. 8 as inverse isochron plots of ^{36}Ar/^{40}Ar vs. ^{39}Ar/^{40}Ar. For reference are tie-lines (dashed) between air and the 85 ka ^{39}Ar/^{40}Ar values appropriate for the irradiation conditions (J values) of each sample. If the samples behaved ideally, the step-heating results would plot along these 85 ka reference lines. Instead, step-heating results that yield statistically permissible apparent ages (open circles) plot below the 85 ka reference line with generally greater deviance at greater ^{39}Ar/^{40}Ar. This increasing divergence lowers the ^{39}Ar/^{40}Ar intercept of a line regressed through the selected results (dotted), leading to a greater apparent age for the samples.

Undegassed melt inclusions remaining in the plagioclase separates may account for the systematic displacement of points down from the 85 ka inverse isochron, producing erroneously old apparent ages (Fig. 9). Lacking initial Ar, pure plagioclase and fully degassed but subsequently undisturbed melt would plot at ^{36}Ar/^{40}Ar of zero and with a ^{39}Ar/^{40}Ar appropriate for the time elapsed after cooling below the closure temperature (for the irradiation conditions of the experiment). Magmatic gases screened for low atmospheric contamination (^{3}He/^{4}He > 5 R/R$_A$, where R$_A$ is the atmospheric ratio) have ^{40}Ar/^{36}Ar values that can exceed 10,000 (Abedini et al., 2006), and so would plot at nearly zero ^{36}Ar/^{40}Ar and zero ^{39}Ar/^{40}Ar. Inclusions of pristine magmatic vapor would plot coincident with this magmatic vapor component, whereas undegassed melt inclusions would plot along a tie-line from this to the pure plagioclase and the identical (theoretical) position of fully degassed and subsequently undisturbed melt. This tie line is another inverse isochron that would be measured in the absence of any interaction with atmospheric Ar. Contamination of the plagioclase separates by undegassed melt inclusions would pull heating-step results off the air-intercept inverse isochron toward the field of undegassed melt inclusions. If various melt inclusions have similar concentrations of dissolved excess Ar, they would plot in a narrow region along this second, non-air intercept inverse isochron. Because glass in the dacite of Sunset Amphitheater is 10 times richer in K than is the plagioclase, the presence of only 2% of such melt inclusions would raise the bulk K of a separate by 20% (relative). Such undegassed melt inclusions would also contain the excess Ar component, and it is this coupling of excess Ar with high-K, hence high ^{40}Ar*, in an otherwise low-K host that produces systematic relations between Ar isotopes that can be interpreted as erroneously old apparent plateau and isochron ages. Inclusions of (nearly) pure magmatic vapor, instead, would displace heating step results toward the origin on an inverse isochron plot, and such steps would typically be rejected from plateau and isochron determinations. Following this reasoning, the closer correspondence of the Ketron Island fine plagioclase Ar ages with the 85 ka eruption age would indicate that the finer plagioclase separate contained proportionally fewer melt inclusions. The two size fractions were separated by sieving of plagioclase separated from crushed pumice, but both were HF-treated, removing adhering glass or melt inclusions exposed during crushing; grains in the coarse split have larger interior domains that so have a greater potential to retain glass inclusions. Ellis et al. (2017) present a similar interpretation for apparently "too old" sanidine crystals from the Mesa Falls tuff, Yellowstone, although they attribute the excess Ar to minute fluid inclusions or residing in crystal defects, rather than to undegassed melt inclusions.

Support for contamination by undegassed melt inclusions is given by a systematic positive relation between K/Ca, measured as a byproduct of the Ar isotope determination, and apparent age for individual heating

Table 8
(U-Th)/He small zircon results for composite pumice sample from Sunrise Park Road.

Material	^{232}Th	±	^{238}U	±	^{147}Sm	±	He	±	TAU	Th/U	Raw age	±1σ	Ft	Ft-cor. age	±1σ	Diseq.-corrected age	+	−
	(ng)	(%)	(ng)	(%)	(ng)	(%)	(ncc)	(%)	(%)		(ka)	(ka)		(ka)	(ka)	(ka)		
Gr 7	0.816	2.3	1.25	2.5	0.00487	13	0.0111	2.5	3.3	0.650	63.3	2.1	0.81	77.9	4.7	98.5	5.8	7.6
Gr 10	0.667	2.3	0.866	2.6	0.00220	13	0.00832	2.9	3.6	0.765	66.9	2.4	0.75	88.8	5.5	110.4	8.4	7.5
Gr 11	0.246	2.4	0.408	2.5	0.00153	16	0.00242	7.8	8.1	0.598	42.7	3.5	0.75	56.7	5.4	70.4	6.0	8.5
Gr 1-2	0.263	2.4	0.390	2.6	0.00150	15	0.00322	5.4	5.9	0.670	58.6	3.4	0.73	80.0	6.2	99.7	9.2	8.2
Gr 2-2	0.740	2.3	1.24	2.5	0.00300	9	0.0107	2.5	3.3	0.590	61.8	2.1	0.81	76.4	4.6	95.5	7.5	5.6
Gr 3-2	0.820	2.3	1.35	2.6	0.00533	9	0.0107	2.1	3.1	0.604	57.1	1.8	0.78	72.8	4.3	90.2	7.0	5.0
Gr 4-2[a]	0.544	2.3	0.839	2.6	0.00334	10	0.00969	2.1	3.1	0.643	82.4	2.5	0.75	110	6.5	–	–	–
Gr 5-2	0.214	2.4	0.367	2.6	0.00141	20	0.00266	3.9	4.5	0.580	52.4	2.3	0.74	70.4	4.7	87.5	7.2	6.2
Gr 6-2	0.341	2.4	0.517	2.6	0.00208	17	0.00355	3.1	3.8	0.654	48.8	1.9	0.84	58.2	3.7	70.4	5.0	4.6
Gr 7-2	0.715	2.3	1.30	2.6	0.00548	10	0.00842	2.1	3.1	0.547	47.2	1.5	0.86	55.2	3.2	67.6	4.4	4.3
Gr 8-2	0.241	2.4	0.514	2.6	0.00193	25	0.00343	2.8	3.6	0.466	49.3	1.8	0.82	59.9	3.7	75.4	4.8	5.3
Gr 9-2	0.455	2.4	0.710	2.6	0.00187	20	0.00494	2.7	3.5	0.636	49.7	1.7	0.74	67.5	4.1	83.5	5.3	6.0
Gr 10-2	0.735	2.3	1.17	2.6	0.00233	12	0.00881	2.2	3.1	0.626	54.1	1.7	0.83	65.2	3.9	80.0	5.5	4.9
Gr 11-2	0.931	2.3	1.84	2.5	0.00257	16	0.0176	2.1	3.1	0.503	70.5	2.2	0.85	82.9	4.9	107.1	8.3	6.6
Gr 12-2	1.981	1.4	3.22	1.9	0.01174	5	0.0305	1.2	2.0	0.611	68.2	1.4	0.85	80.5	4.3	103.0	5.5	7.2
Gr 13-2	0.259	1.4	0.367	2.0	0.00159	17	0.00284	1.2	2.2	0.699	54.5	1.2	0.80	68.5	3.7	82.7	6.0	3.8
Gr 14-2	0.751	1.4	1.34	1.9	0.00332	11	0.0097	1.2	2.1	0.555	52.4	1.1	0.79	66.5	3.6	83.5	4.5	5.6

Notes: sample collected at latitude 46.9036, longitude −121.5908; TAU = total analytical uncertainty; Gr gives grain number.
[a] Excluded from average; disequilibrium corrected age is based on individually calculated D_{230} values (from zircon and whole-rock Th/U) and an average crystallization age of 147 ± 8 ka.

steps for the Ketron Island plagioclase separates (Fig. 10). Nearly all heating-step results for the Ketron Island plagioclase separates have derived K/Ca from 0.059 to 0.075, with a corresponding increase in apparent age (age assuming an air ^{40}Ar/^{36}Ar intercept) from 85 to 270 ka. The correlation of apparent age with K/Ca identifies the excess Ar as coupled with a K-rich, Ca-poor component, such as glass. Addition of 1.5 to 4.5 wt% of the average glass (K/Ca: 3.4) to the average plagioclase rim (K/Ca: 0.052) would account for the K/Ca range of the heating steps. Shown for comparison are the K/Ca versus apparent age results for the probable lithic-derived altered plagioclase from Sunset Amphitheater previously, but erroneously, interpreted as dating the pumice eruption.

6.2. Geological significance of the 85 ka eruption age

The 85 ± 6 ka (U-Th)/He zircon age for the dacite of Sunset Amphitheater confirms eruption after the penultimate glaciation (MIS 6) and before the last glacial maximum (MIS 2), consistent with Crandell and Miller's (1974) assignment of the underlying and overlying tills along the Sunrise Park Road to the Hayden Creek and Evans Creek Drifts. Crandell and Miller (1974) noted that the pumice is also exposed in Pleistocene stream deposits shortly below the Sunrise Park road, and that the height of those deposits above the valley floor indicates that a glacier then partly filled the valley of the White River. In detail, the age identifies the eruption as having been during MIS 5a or 5b that

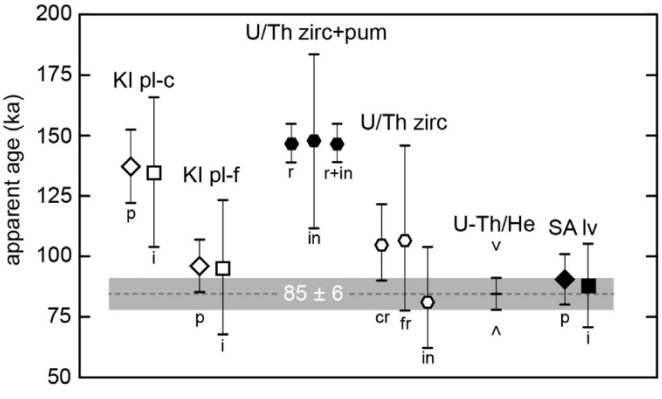

Fig. 7. Summary of age results for the dacite of Sunset Amphitheater and associated rocks. Diamonds and squares are ^{40}Ar/^{39}Ar plateau (p) and isochron (i) ages with 2σ uncertainty brackets for plagioclase (open symbols) from Ketron Island pumice coarse (KI pl-c), Ketron Island pumice fine (KI pl-f), and for groundmasses of Sunset Amphitheater lava near the level of the pumice band (filled symbols, SA lv). Zircon U-Th model ages are shown as hexagons, filled for isochron results constrained to pass through bulk tephra, and open where regressed solely through zircon analyses. Tephra-constrained zircon U-Th model ages are subdivided into interiors (in), rims (r), and combined (r + in). Unconstrained zircon U-Th model ages are shown for coarse-grain rims (cr), fine-grain rims (fr), and coarse-grain interiors (in). (U-Th)/He results are shown as a simple bar with 2σ uncertainty brackets, and also are depicted as a dashed line and gray field. Limiting unpreferred (U-Th)/He age solutions for instantaneous growth and eruption and for complete U-series equilibrium are shown as ∨ and ∧ symbols.

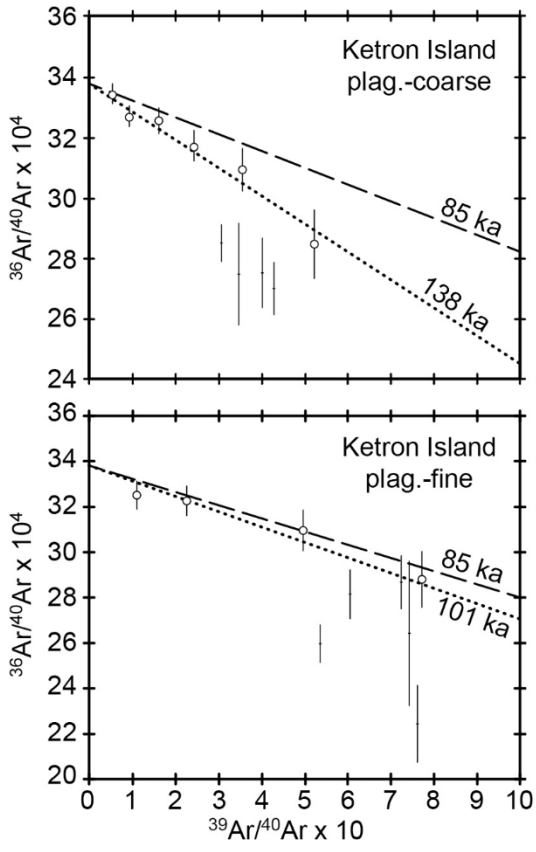

Fig. 8. Inverse isochron ^{40}Ar/^{39}Ar plots for plagioclase separated from pumice collected at Ketron Island. Heating-step results yielding statistically permissible ages are shown as white circles with 2σ uncertainty brackets. Rejected steps are shown as simple 2σ uncertainty brackets. For reference are eruption-age 85 ka inverse isochrons passing through air ^{36}Ar/^{40}Ar (dashed lines), as well as inverse isochrons and corresponding ages regressed through the selected heating step results (dotted lines).

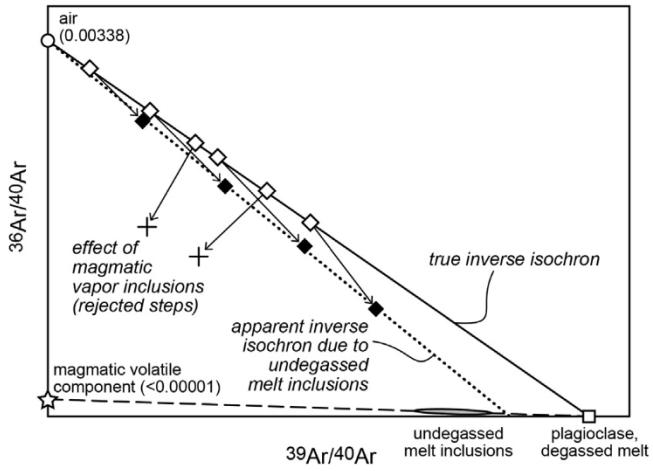

Fig. 9. Inverse isochron $^{40}Ar/^{39}Ar$ diagram showing the effect of undegassed melt inclusions on plagioclase step-heating results. Pure plagioclase lacking both melt inclusions and air-derived Ar would plot as the open square, as would (fictive) fully degassed but subsequently undisturbed melt (glass). Heating-step results that released combinations of air-derived Ar ($^{36}Ar/^{40}Ar$: 0.00338) and radiogenic Ar produced solely after eruption would plot along the true inverse isochron (solid black line) and are depicted as open diamonds. A magmatic volatile component, present dissolved in melt, as bubbles, or both, would plot near the origin ($^{36}Ar/^{40}Ar < 0.00001$, $^{39}Ar/^{40}Ar = 0$) and is shown as a star. Undegassed melt inclusions would plot along an inverse isochron between the magmatic volatile component and plagioclase or (fictive) fully degassed melt. Release of Ar from undegassed melt inclusions pulls plagioclase – air-Ar mixtures off the true inverse isochron toward the Ar values of undegassed melt inclusions, yielding an erroneously old apparent inverse isochron, shown as a dotted line. Release of Ar from (nearly) pure bubbles of magmatic vapor would displace step-heating results toward the origin (pluses), and such results would be rejected in the construction of Ar plateaus and isochrons.

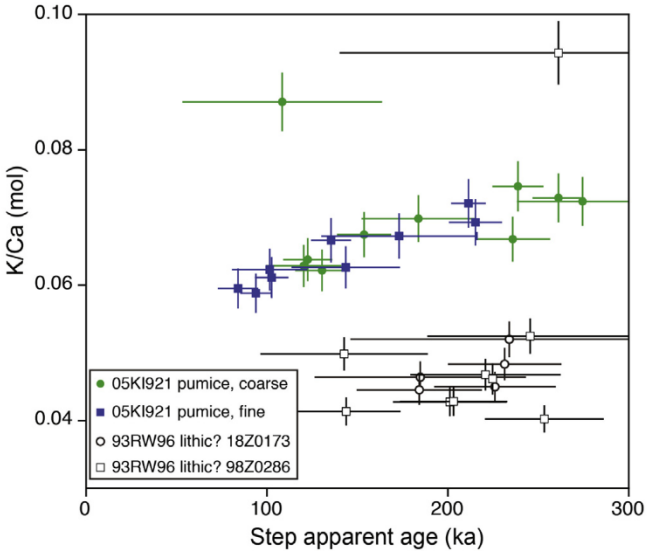

Fig. 10. K/Ca vs. apparent age (ka) for individual heating steps of pumice plagioclase from Ketron Island sample 05KI921 and probable lithic-derived plagioclase from Sunset Amphitheater bulk tephra sample 93RW96 with 1-sigma uncertainty brackets. Apparent age is derived assuming an atmospheric excess argon composition and equals the age for the heating step on a conventional $^{40}Ar/^{39}Ar$ plateau diagram (Fig. 4).

were part of a protracted period of irregularly increasing global ice volume following the strong interglacial of MIS 5e, leading into the moderate and strong glacials of MIS 4 and 2 (Fig. 11). Global sea level was 20 m to 30 m lower than Holocene values during MIS 5a and may have reached 60 m below the Holocene in MIS 5b (Lambeck et al., 2002). Our new zircon (U-Th)/He age corrects the former erroneous assignment of the Ketron Island exposure to MIS 7 (Walsh et al., 2003b). The pumice-rich sands exposed at Ketron Island overlie gravels interpreted by Walsh et al. (2003b) as deposits of energetic streams associated with the Cordilleran ice sheet. The new age determination for the pumice is consistent with those gravels having been deposited during MIS 6, or during the retreat of ice into strongly interglacial MIS 5e, and would correlate those gravels with the Double Bluff Drift of the northern Puget Lowland (Booth et al., 2003; Porter, 2004). The Cordilleran ice sheet advanced twice following eruption of the dacite of Sunset Amphitheater, first producing the Possession Drift during MIS 4, and then producing the more extensive Vashon Drift during MIS 2. The Possession Drift has not been identified as far south as Ketron Island, but any associated sediments should be sought above the level of the pumiceous sand deposit.

The presence of strong hydrothermal alteration in rocks below the prominent unconformity in Sunset Amphitheater Headwall and the absence of alteration above the unconformity was interpreted by John et al. (2008) as evidence for an episode of widespread alteration prior to ~194 ka. The 85 ka eruption age for the pumice, however, shows that the alteration may have continued or took place later. The marginal etching, clay coatings, and calcite of the plagioclase separate erroneously first dated as the dacite of Sunset Amphitheater is evidence for hydrothermal activity within the edifice after ~200 ka.

7. Conclusions

(U-Th)/He zircon geochronology of a major pumiceous fall deposit from Mount Rainier, the dacite of Sunset Amphitheater, establishes an eruption age as 85 ± 6 ka. This date is resolvably younger than $^{40}Ar/^{39}Ar$ apparent ages on plagioclase phenocrysts, and of zircon surface and interior U-Th zircon model ages. The anomalously old $^{40}Ar/^{39}Ar$ apparent ages are ascribed to the presence of traces of undegassed melt inclusions in the plagioclase separates that would be rich in both post-eruptive radiogenic ^{40}Ar and in initial excess Ar. A preferred 147 ka U-Th disequilibria model age for zircon crystallization is near the end of a major period of growth of the Rainier edifice, a time when general cooling of the roots of the volcanic system would be expected.

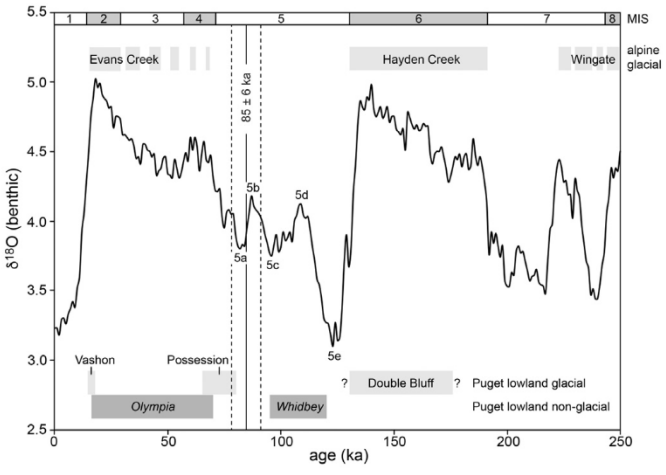

Fig. 11. Late Pleistocene and Holocene marine benthic $\delta^{18}O$, MIS stages, and selected substages (Lisiecki and Raymo, 2005). Solid and dashed vertical lines mark the preferred age and ±2σ uncertainty window for eruption of the dacite of Sunset Amphitheater. Approximate age spans of southwestern Washington alpine glacial drifts (Evans Creek, Hayden Creek, Wingate Hill) are shown as light gray bars at the top of the diagram. Evans Creek glaciers reached their greatest extents during MIS 2, but ridge-capping ice-marginal lava flows at Mt. Rainier show that alpine glaciers were also enlarged during much of MIS 3, 4, and 5. Glacial deposits in the Puget Lowland resulting from advances of the Cordilleran ice sheet are shown as light gray bars in the lower part of the diagram (Vashon, Possession, Double Bluff), along with intervening non-glacial deposits (Olympia, Whidbey). Possession Drift has not been identified as far south as Ketron Island. Ages for glacial and non-glacial deposits are generalized from Booth et al. (2003), Porter (2004), McCormack and Troost (2016), and Easterbrook (2016), converted to calendar years from ^{14}C ages.

The 85 ka eruption age provides an important marker for understanding the glacial history of the Puget Basin. Since Willis (1897), the Puget Basin has been recognized as having been overrun by Pleistocene ice, and although drift deposits are exposed widely in shorefront bluffs, all but the Vashon Drift (MIS 2) are generally too old to date by ^{14}C. The refined age for the dacite of Sunset Amphitheater confidently identifies the gravels below the Ketron Island pumiceous sand exposure as having been deposited during MIS 6, or as ice retreated into MIS 5e, equivalent to the Double Bluff Drift of northern Puget Sound. Any deposits associated with the ice advance that produced the Possession Drift of northern and central Puget Sound must lie above the level of the Ketron Island pumiceous sands. Tills along the northeast foot of the Mount Rainier were correctly assigned to the Evans Creek (MIS 2) and Hayden Creek (MIS 6) Drifts (Crandell and Miller, 1974).

Acknowledgements

The USGS electron-microprobe laboratory was maintained by Mr. Robert Oscarson and Dr. Leslie O'Brien. Sample preparation and mineral separates for Ar geochronology were performed by Dean Miller and James Saburomaru. M.D. was supported by the Australian Research Council (ARC) Discovery funding scheme (DP160102427) and Curtin Research Fellowship. The ion microprobe facility at UCLA is partly supported by a grant from the Instrumentation and Facilities Program, Division of Earth Sciences, National Science Foundation. Determination of U-Th isotopic compositions was supported by the Science Vanguard Research Program of the Ministry of Science and Technology (MOST) (107-2119-M-002-051 to C.-C.S.), the National Taiwan University (105R7625 to C.-C.S.), and the Higher Education Sprout Project of the Ministry of Education, Taiwan ROC (107L901001 to C.-C.S.). We thank Mark Stelten, Seth Burgess, José Luis Arce, and Chris Conway for their constructive suggestions, and Tim Walsh for boat access to Ketron Island. Any use of trade, firm, or product names is for descriptive purposes only and does not imply endorsement by the U.S. Government.

References

Abedini, A., Hurwitz, S., Evans, W.C., 2006. USGS-NoGasDat – a global dataset of noble gas concentrations and their isotopic ratios in volcanic systems. U.S. Geol. Surv. Data Series 202. https://pubs.usgs.gov/ds/2006/202.

Ankney, M.E., Johnson, C.M., Bacon, C.R., Beard, B.L., Jicha, B.R., 2013. Distinguishing lower and upper crustal processes in magmas erupted in the buildup to the 7.7 ka climactic eruption of Mount Mazama, Crater Lake, Oregon, using 238U-230Th disequilibria. Contrib. Mineral. Petrol. 166, 563–585.

Armstrong, J.T., 1995. CITZAF: a package of correction programs for quantitative electron microbeam X-ray analysis of thick polished materials, thin films, and particles. Microbeam Anal. 4, 177–200.

Avellán, D.R., Macías, J.L., Arce, J.L., Jiménez-Haro, A., Saucedo-Girón, R., Garduño-Monroy, V.H., Sosa-Ceballos, G., Bernal, J.P., López-Loera, H., Cisneros, G., Layer, P.W., 2018. Eruptive chronology and tectonic context of the late Pleistocene Tres Vírgenes volcanic complex, Baja California Sur (México). Jour. Volcanol. Geotherm. Res. 360, 100–125.

Bacon, C.R., 1986. Magmatic inclusions in silicic and intermediate volcanic rocks. Jour. Geophys. Res. 91, 6091–6112.

Baedecker, P.A., 1987. Methods for geochemical analysis – analytical methods used in the Geologic Division laboratories of the U.S. Geological Survey for the inorganic chemical analyses of rock and mineral samples. U.S. Geol. Surv. Bull. 1770.

Blundy, J., Wood, B., 2003. Mineral-melt partitioning of uranium, thorium, and their daughters. In: Bourdon, B., Henderson, G.M., Lundstrom, C.C., Turner, S.P. (Eds.), Uranium-series geochemistry. Rev. Mineral 52, pp. 59–118.

Booth, D.B., Troost, K.G., Clague, J.J., Waitt, R.B., 2003. The cordilleran ice sheet. Devel. Quatern. Sci. 1, 17–43.

Calvert, A.T., Moore, R.B., McGimsey, R.G., 2005, Argon geochronology of Late Pleistocene to Holocene Westdahl Volcano, Unimak Island, Alaska. U.S. Geol. Surv. Prof. Paper 1709-D, 16 pp.

Carey, S., Gardner, J., Sigurdsson, H., 1995. The intensity and magnitude of Holocene plinian eruptions from Mount St. Helens volcano. Jour. Volcanol. Geotherm. Res. 66, 185–202.

Cheng, H., Edwards, R.L., Shen, C.-C., Polyak, V.J., Asmerom, Y., Woodhead, J., Hellstrom, J., Wang, Y., Kong, X., Spötl, C., 2013. Improvements in ^{230}Th dating, ^{230}Th and ^{234}U half-life values, and U-Th isotopic measurements by multi-collector inductively coupled plasma mass spectroscopy. Earth Planet. Sci. Lett. 371–372, 82–91.

Clark, P.U., Dyke, A.S., Shakun, J.D., Carlson, A.E., Clark, J., Wohlfarth, B., Mitrovica, J.X., Hostetler, S.W., McCabe, A.M., 2009. The last glacial maximum. Science 325, 710–714.

Coble, M.A., Burgess, S., Klemetti, E.K., 2017. New zircon (U-Th)/He and U/Pb eruption age for the Rockland tephra, western USA. Quatern. Sci. Rev. 172, 109–117.

Crandell, D.R., 1969, Surficial geology of Mount Rainier National Park, Washington. U.S. Geol. Surv. Bull. 1288, 41 pp.

Crandell, D.R., Miller, R.D., 1974, Quaternary stratigraphy and extent of glaciation in the Mount Rainier region, Washington. U.S. Geol. Surv. Prof. Paper 847, 59 pp.

Dalrymple, G.B., Moore, J.G., 1968. Argon-40: excess in submarine pillow basalts from Kilauea Volcano, Hawaii. Science 161, 1132–1135.

Danišík, M., Shane, P., Schmitt, A.K., Hogg, A., Santos, G.M., Storm, S., Evans, N.J., Fifield, L.K., Lindsay, J.M., 2012. Re-anchoring the late Pleistocene tephrochronology of New Zealand based on concordant radiocarbon ages and combined $^{238}U/^{230}Th$ disequilibrium and (U–Th)/He zircon ages. Earth Planet. Sci. Lett. 349, 240–250.

Danišík, M., Schmitt, A.K., Stockli, D.F., Lovera, O.M., Dunkl, I., Evans, N.J., 2017. Application of combined U-Th-disequilibrium/U-Pb and (U-Th)/He zircon dating to tephrochronology. Quatern. Geochron. 40, 23–32.

Easterbrook, D.J., 2016. Late Quaternary glaciation of the Puget Lowland, North Cascade Range, and Columbia Plateau, Washington. In: Cheney, E.S. (Ed.), The Geology of Washington and Beyond, From Laurentia to Cascadia. University of Washington Press, Seattle, pp. 257–286.

Ellis, B.S., Mark, D.F., Troch, J., Bachmann, O., Guillong, M., Kent, A.J.R., von Quadt, A., 2017. Split-grain $^{40}Ar/^{39}Ar$ dating: integrating temporal and geochemical data. Chem. Geol. 45, 15–23.

Farley, K.A., Kohn, B.P., Pillans, B., 2002. The effects of secular disequilibrium on (U–Th)/He systematics and dating of Quaternary volcanic zircon and apatite. Earth Planet. Sci. Lett. 201, 117–125.

Fiske, R.S., Hopson, C.A., and Waters, A.C., 1963, Geology of Mount Rainier National Park, Washington. U.S. Geological Surv. Prof. Paper 444, 93 pp.

Fleck, R.J., Calvert, A.T., 2016. Intercalibration of $^{40}Ar/^{39}Ar$ mineral standards with Bodie Hills sanidine. Geol. Soc. Am. Abstr. Programs 48. https://doi.org/10.1130/abs/2016AM-286011.

Ghiorso, M.S., Evans, B.W., 2008. Thermodynamics of rhombohedral oxide solid solutions and a revision of the Fe–Ti two-oxide geothermometer and oxygen-barometer. Amer. Jour. Sci. 308, 957–1039.

Harrison, T.M., Watson, E.B., 1983. Kinetics of zircon dissolution and zirconium diffusion in granitic melts of variable water content. Contrib. Mineral. Petrol. 84, 66–72.

Jicha, B.R., Johnson, C.M., Hildreth, W., Beard, B.L., Hart, G.L., Shirey, S.B., Singer, B.S., 2009. Discriminating assimilants and decoupling deep- vs. shallow-level crystal records at Mount Adams using 238U-230Th disequilibra and Os isotopes. Earth Planet. Sci. Lett. 277, 38–49.

John, D.A., Sisson, T.W., Breit, G.N., Rye, R.O., Vallance, J.W., 2008. Characteristics, extent and origin of hydrothermal alteration at Mount Rainier volcano, Cascade arc, USA: implications for debris-flow hazards and mineral deposits. Jour. Volcanol. Geotherm. Res. 175, 289–314.

Johnson, D.M., Hooper, P.R., Conrey, R.M., 1999. XRF analysis of rock and minerals for major and trace elements on a single low dilution Li-tetraborate fused bead. Adv. X-ray Anal. 41, 843–867.

Kelley, S., 2002. Excess argon in K-Ar and Ar-Ar geochronology. Chem. Geol. 188, 1–22.

Lambeck, K., Esat, T.M., Potter, E.-K., 2002. Links between climate and sea levels for the past three million years. Nature 419, 199–206.

Lescinsky, D.T., Sisson, T.W., 1998. Ridge-forming, ice-bounded lava flows at Mount Rainier. Washington. Geol. 26, 351–354.

Lisiecki, L.E., Raymo, M.E., 2005, A Plio-Pleistocene stack of 57 globally distributed benthic $\delta^{18}O$ records. Paleoceanography 20, PA1003, doi:https://doi.org/10.1029/2004PA001071.

Matthews, N.E., Vazquez, J.A., Calvert, A.T., 2015. Age of the Lava Creek supereruption and magma chamber assembly at Yellowstone based on $^{40}Ar/^{39}Ar$ and U-Pb dating of sanidine and zircon crystals. Geochem. Geophys. Geosys. 16, 2508–2528.

McCormack, D.H., Troost, K.G., 2016. Quaternary geology of northwestern King County and southwestern Snohomish County, Washington. In: Cheney, E.S. (Ed.), The Geology of Washington and Beyond, From Laurentia to Cascadia. University of Washington Press, Seattle, pp. 287–310.

Morgan, G.B., London, D., 1996. Optimizing the electron microbeam analysis of alkali aluminosilicate glasses. Am. Mineral. 81, 1176–1185.

Mullineaux, D.R., 1974, Pumice and other pyroclastic deposits in Mount Rainier National Park, Washington. U.S. Geol. Surv. Bull. 1326, 83 pp.

Nakada, S., Bacon, C.R., Gartner, A.E., 1994. Origin of phenocrysts and compositional diversity in pre-Mazama rhyodacite lavas, Crater Lake. Oregon. Jour. Petrol. 35, 127–162.

Nathenson, M., 2017. Revised tephra volumes for Cascade Range volcanoes. Jour. Volc. Geotherm. Res. 341, 42–52.

Newman, S., Macdougall, J.D., Finkel, R.C., 1986. Petrogenesis and ^{230}Th-^{238}U disequilibrium at Mt. Shasta, California, and the Cascades. Contrib. Mineral. Petrol. 93, 195–206.

O'Neill, H.St.C., Pownceby, M.I., 1993. Thermodynamic data from redox reactions at high temperatures. I. An experimental and theoretical assessment of the electrochemical method using stabilized zirconia electrolytes, with revised values for the Fe-"FeO", Co-CoO, Ni-NiO and Cu-Cu_2O oxygen buffers, and new data for the W-WO_2 buffer. Contrib. Mineral. Petrol. 114, 296–314.

Porter, S.C., 2004. Glaciation of western Washington, U.S.A., in Ehlers, J., and Gibbard, P.L., eds., Quaternary Glaciations – Extent and Chronology. Dev. Quaternary Sci. 2 (B), 289–293.

Ratajeski, K., 1999, Field, geochemical, and experimental study of mafic to felsic plutonic rocks associated with the intrusive suite of Yosemite Valley, California. Ph.D. thesis, University of North Carolina, Chapel Hill, 196 pp.

Reagan, M.K., Sims, K.W.W., Erich, J., Thomas, R.B., Cheng, H., Edwards, R.L., Layne, G., Ball, L., 2003. Time-scales of differentiation from mafic parents to rhyolite in North American continental arcs. Jour. Petrol 44, 1703–1726.

Reid, M.R., Coath, C.D., Harrison, T.M., McKeegan, K.D., 1997. Prolonged residence times for the youngest rhyolites associated with Long Valley caldera: ^{230}Th-^{238}U ion microprobe dating of young zircons. Earth Planet. Sci. Lett. 150, 27–39.

Reiners, P.W., Spell, T.L., Nicolescu, S., Zanetti, K.A., 2004. Zircon (U-Th)/He thermochronometry: He diffusion and comparisons with $^{40}Ar/^{39}Ar$ dating. Geochim. Cosmochim. Acta 68, 1857–1887.

Rubatto, D., Hermann, J., 2007. Experimental zircon/melt and zircon/garnet trace element partitioning and implications for geochronology of crustal rocks. Chem. Geol. 241, 38–61.

Schmitt, A.K., 2011. Uranium series accessory crystal dating of magmatic processes. Ann. Rev. Earth Plant. Proc. 39, 321–349.

Schmitt, A.K., Stockli, D.F., Niedermann, S., Lovera, O.M., Hausback, B.P., 2010. Eruption ages of Las Tres Vírgenes volcano (Baja California): a tale of two helium isotopes. Quaternary Geochron. 5, 503–511.

Schmitt, A.K., Martin, A., Stockli, D.F., Farley, K.A., 2012. (U-Th)/He zircon and archeological ages for a late prehistoric eruption in the Salton Trough (California, USA). Geology 41, 7–10.

Schmitz, M.D., Bowring, S.A., Ireland, T.R., 2003. Evaluation of Duluth Complex anorthositic series (AS3) zircon as a U-Pb geochronological standard: New high-precision isotope dilution thermal ionization mass spectrometry results. Geochim. Cosmochim. Acta 67, 3665–3672.

Shen, C.-C., Cheng, H., Edwards, R.L., Moran, S.B., Edmonds, H.N., Hoff, J.A., Thomas, R.B., 2003. Measurement of attogram quantities of ^{231}Pa in dissolved and particulate fractions of seawater by isotope dilution thermal ionization mass spectroscopy. Anal. Chem. 75, 1075–1079.

Shen, C.-C., Wu, C.-C., Cheng, H., Edwards, R.L., Hsieh, Y.-T., Gallet, S., Chang, C.-C., Li, T.-Y., Lam, D.D., Kano, A., Hori, M., Spötl, C., 2012. High-precision and high-resolution carbonate ^{230}Th dating by MC-ICP-MS with SEM protocols. Geochim. Cosmochim. Acta 99, 71–86.

Sisson, T.W., Vallance, J.W., 2009. Frequent eruptions of Mount Rainier over the last ~2,600 years. Bull. Volcanol. 71, 595–618.

Sisson, T.W., Vallance, J.W., Pringle, P.T., 2001, Progress made in understanding Mount Rainier's hazards. EOS Trans. Amer. Geophys. Union 82, 8 pp, doi:https://doi.org/10.1029/01EO00057.

Sisson, T.W., Salters, V.J.M., Larson, P.B., 2014. Petrogenesis of Mount Rainier andesite: Magma flux and geologic controls on the contrasting differentiation styles at stratovolcanoes of the southern Washington Cascades. Geol. Soc. Amer. Bull. 126, 122–144. https://doi.org/10.1130/B30852.1.

Steiger, R.H., Jager, E., 1977. Subcommission on geochronology: convention on the use of decay constants in geo- and cosmochronology. Earth Planet. Sci. Lett. 36, 359–362.

Thornber, C.R., Pallister, J.S., Lowers, H.A., Rowe, M.C., Mandeville, C.W., Meeker, G.P., 2008. Chemistry, mineralogy, and petrology of amphibole in Mount St. Helens 2004-2006 dacite, in Sherrod, D.S., Scott, W.E., Stauffer, P.H., eds. U.S. Geol. Surv. Prof. Paper 1750, 727–754.

Walsh, T.J., Polenz, M., Logan, R.L., 2003a. Geologic map of the McNeil Island 7.5-minute quadrangle, Pierce and Thurston Counties, Washington. Wash. Div. Geol. Earth Res. Open File Report 2003-22.

Walsh, T.J., Polenz, M., Logan, R.L., Lanphere, M.A., Sisson, T.W., 2003b. Pleistocene tephrostratigraphy and paleogeography of Southern Puget Sound near Olympia, Washington. In: Swanson, T.W. (Ed.), Western Cordillera and Adjacent Areas. Geol. Soc. Amer. Field Guide 4, pp. 225–236.

Wiedenbeck, M., Alle, P., Corfu, F., Griffin, W.L., Meier, M., Oberli, F., von Quadt, A., Roddick, J.C., Spiegel, W., 1995. Three natural zircon standards for U-Th-Pb, Lu-Hf, trace element, and REE analyses. Geostand. Newslett. 19, 1–23.

Willis, B., 1897. Drift phenomena of Puget Sound. Geol. Soc. Amer. Bull. 9, 111–162.

Wright, H.M., Vazquez, J.A., Champion, A.T., Calvert, A.T., Mangan, M.T., Stelten, M., Cooper, K.M., Herzig, C., Schriener Jr., A., 2015. Episodic Holocene eruption of the Salton Buttes rhyolite, California, from paleomagnetic, U-Th, and Ar/Ar dating. Geochem. Geophys. Geosys. 16, 1198–1210.